Università di Foggia

Department of Clinical and Experimental Medicine

PhD Thesis
Basic and Clinal Neuroscience
XXXVIII Cycle

Circadian control of mitochondria OXPHOS activity, dynamics and turnover *in vitro* synchronized cells

TUTOR
Prof.ssa Rosella Scrima

PHD CANDIDATE
Michela Rosiello

Academic year 2024/2025

ABSTRACT

Circadian rhythms driven by biological clocks regulate physiological processes in all living organisms by anticipating daily geophysical changes, thus enhancing environmental adaptation. The cellular time-keeping mechanism is controlled by a transcription-translation feedback loop involving a set of well-characterized transcription factors (with BMAL1/CLOCK being the master circadian clock transcription factors). This mechanism controls 50-60% of genes expressed in mammals including those that regulate cell metabolism. In previous studies, in an in-vitro synchronized cell model, we showed a temporal oscillation of the mitochondrial respiratory chain activity coupled to the ATP synthesis. This observation has been recently confirmed in a panel of different cell types (both primary and cancer-derived lines) indicating this as a general phenomenon. Notably, while primary cell types exhibited similar rhythmic respiratory profiles, cancer-derived cell lines displayed highly heterogeneous rhythmic changes highlighting the need for personalized chronotherapy. The mtDNA genes coding for respiratory chain complex subunits as well as of factors regulating mitochondrial dynamics and turnover revealing for all a BMAL-1-dependent rhythmic profile. Careful analysis of the oscillation phases, supported by confocal microscopy imaging, points to a balance between mitochondrial biogenesis and degradation to optimize the organelle functions.

1. INTRODUCTION

1.1 Circadian Clock

Life is a cyclical phenomenon. It consists of birth and death, annual cycles, seasonal cycles, lunar cycles, daily cycles, or more commonly known as circadian cycles.

Most of the organisms of Earth are subjected to circadian rhythms.

Circadian rhythm refers to an innate, endogenous, and entrainable rhythm whose cycle is approximately 24 hours. The term “circadian,” derived from the Latin “circa diem” meaning “about a day.

This rhythm is retained under constant conditions, in the absence of any external or environmental cue that entrains the circadian clock (referred to as zeitgebers), including light, temperature, eating patterns, exercise, and social interactions.[1]

During evolution the organisms developed autonomous time-keeping mechanisms enabling them to anticipate the geo-physical diurnal changes thereby acquiring a competitive advantage.[2]

Therefore, light is the external stimulus that is most closely related to daily circadian cycles and the most visually tangible.

In mammals, photic environmental cues are perceived by melanopsin-containing retinal ganglion cells that convey their outputs to the suprachiasmatic nuclei (SCN) of the hypothalamus directly via the retinohy pothalamic tract (RHT), whose main neurotransmitter is the excitatory amino acid glutamate. The signal then passes directly to the suprachiasmatic nucleus (SCN).[3]

The SCN receives direct retinal innervation via the retinohypothalamic tract (RHT) to ensure its synchronization to day–night cycles. The SCN clock projects to various brain centres, many of which contain local circadian clocks that direct behavioural (for example, feeding–fasting and sleep wakefulness), autonomic and neuroendocrine circadian rhythms. These systemic cues synchronize the local molecular clocks of peripheral tissues,

and these local clocks in turn direct local programs of circadian gene expression that regulate physiological rhythms critical to health (for example, rhythms relating to mental alertness, blood pressure, triglyceride metabolism and renal function.[4]

The SCN determine circadian period that is reported in normal subjects to be on average 24.2 to 24.5 h in the absence of light cues, whereas in blind individuals, who do not have a functioning retina or retinohypothalamic tract, the circadian period can range from 23 to 25 h.[3]

The SCN is necessary for circadian behaviour: its compromise by surgical ablation in animals and by pituitary tumours or vascular disease in humans disrupts daily rhythms. It is also sufficient for circadian behaviour: grafts of neonatal SCN tissue into SCN-ablated rodents restore rest–activity rhythms.[4]

The SCN clock projects to various brain centres, many of which contain local circadian clocks that direct behavioural, autonomic and neuroendocrine circadian rhythms. These systemic cues synchronize the local molecular clocks of peripheral tissues, and these local clocks in turn direct local programs of circadian gene expression that regulate physiological rhythms critical to health (for example, rhythms relating to mental alertness, blood pressure, triglyceride metabolism1 and renal function.[4]

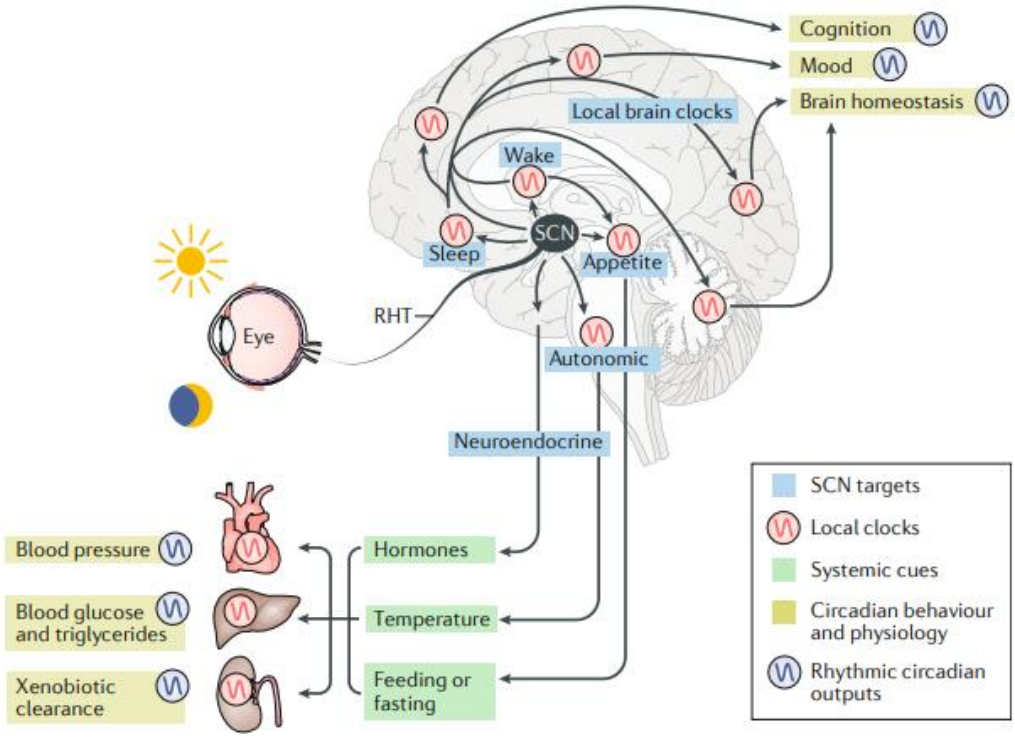

Figure 1: Local clock and organism activities regulated by suprachiasmatic nucleus (SCN) among sleep, wakefulness, appetite, blood pressure, body temperature, blood glucose, triglyceride levels, etc.

In everyday life, circadian rhythm plays a crucial role in maintaining physiological and behavioral balance. However, in modern society, individuals frequently make unconscious choices, often driven by necessity, that disregard the intrinsic programming of the internal clock. Consequently, our biological rhythms may become desynchronized from the external environment, and if not properly realigned, this misalignment can lead to adverse health outcomes.

Circadian misalignment, which encompasses factors such as feeding behavior, sleep patterns, and the light/dark cycle disrupts the homeostatic regulation of these processes, resulting in internal disequilibrium. This disruption has been identified as a contributing feature of several pathological conditions, ranging from metabolic syndrome to cancer.

Conversely, proper alignment and internal synchronization of the circadian clock have been shown to mitigate tissue dysfunction and promote overall well-being. These findings support the notion that circadian biology is an

innate, evolutionarily conserved system so circadian rhythms are intrinsically generated and genetically encoded.[5]

1.1.1 Clock genes

Almost half of all protein-coding genes show circadian-dependent transcription in at least one tissue in humans and rhythmic expression of genes is accomplished through a cell intrinsic transcriptional/translational feedback loop (TTFL).[6]

In mammals, at cellular level, circadian rhythmicity is driven by a gene set known as *clock genes*, which encoded transcription factors forming transcriptional–translational feedback loops.

Primary transcriptional–translational feedback loop (TTFL) is a positive loop composed by Aryl hydrocarbon receptor nuclear translocator-like 1 (*BMAL1*) and Circadian Locomotor Output Cycles Kaput (*CLOCK*). These proteins form a heterodimer that bind enhancer E-box regulatory sequence (5'-CACGTG-3'), and their gene target are Period (*PER1, PER2, PER3*) e Cryptocrome (*CRY1, CRY2*). This gene encoded for PER and CRY protein, which are included in negative loop. They dimerize and act to inhibit transcription of BMAL1.[4,6]

This oscillating mechanism is added to a secondary feedback loop. This loop involves nuclear receptors belonging to the Nuclear Receptor Subfamily 1 Group D member 1,2 (NR1D1,2 commonly known as REV-ERBα, β) and RAR-Related Orphan Receptor (ROR) families. These nuclear receptors linked to the action of core clock oscillator driving the rhythmic expression of BMAL1 from sites known as ROR response element binding sites (RORE binding sites). These intricate feedback loops collectively orchestrate rhythms that occur with a roughly 24-h period.[6]

Mutations in the genes of these nuclear receptors alter the amplitude and period of activity rhythms, and Rev-erb-double- knockout mice exhibit severely disrupted circadian behaviour.[4]

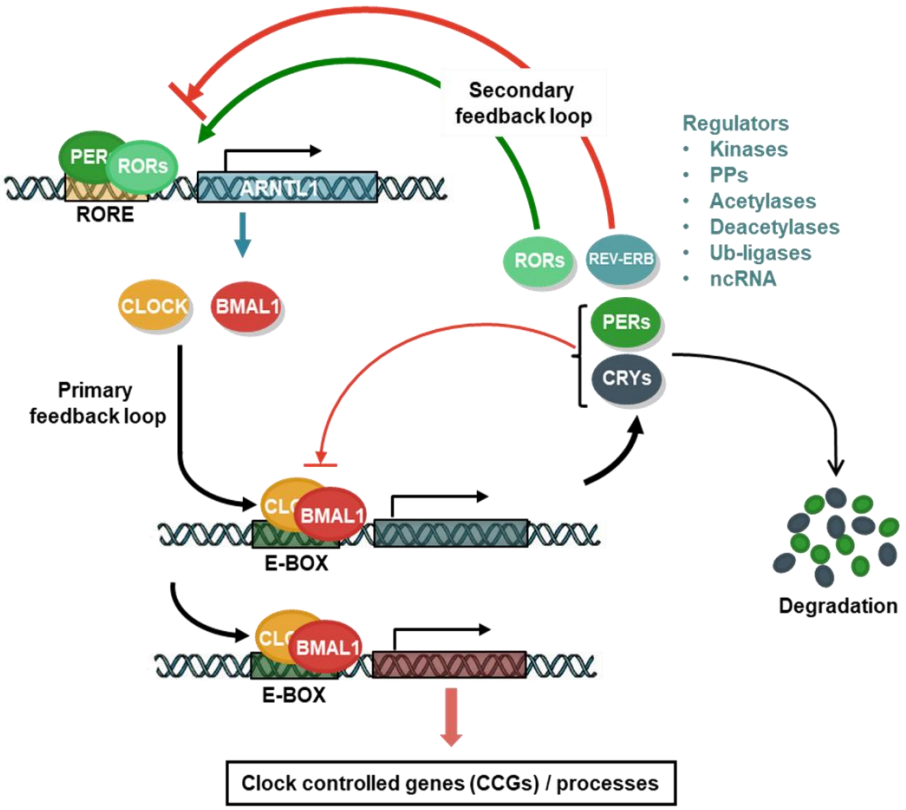

Figure 2: Transcriptional–translational feedback loop (TTFL) with primary and secondary feedback loops and main clock genes.

A third CLOCK–BMAL1-driven transcriptional loop involves the PAR-bZip (proline and acidic amino acid-rich basic leucine zipper) factors DBP (D-box binding protein), TEF (thyrotroph embryonic factor) and HLF (hepatic leukaemia factor) with repressor NFIL3 (nuclear factor, interleukin-3 reglated; also known as E4BP4). Together, these three transcriptional feedback loops can generate cycles of transcription with various phases of expression depending on the combination of cis- elements (that is, E-boxes, ROREs and D-boxes) in the promoters and enhancers of specific target genes[7].

1.2 Clock genes and metabolism

Metabolism is the network of biochemical reactions that organisms employ to transform molecules with the purpose of generating energy and structural building blocks.

Fundamental principles of metabolic regulation are highly conserved in all forms of life, and metabolic control transcends every aspect of cellular physiology, from the beginning of life to its end.

Discrepancies between the metabolic requirements and the metabolic capacity of an organism are associated with a wide variety of pathologies, including metabolic syndrome and type 2 diabetes.[8]

The entire human body, and thus every organ, is subject to circadian rhythms. External light inputs regulate SCN, which in turn controls the expression of clock genes. The neural and endocrine signals produced by the central clock then regulate peripheral clocks located in the liver, pancreas, adipose tissue, stomach, and intestine. These organs participate in processes such as glucose and lipid metabolism and nutrient absorption, which therefore occur in a rhythmic manner.

In addition to light, hunger also stimulates the transcription of clock genes. Nutritional status conveys signals from peripheral clocks to the central clock through proteins such as SIRT1 and AMPK, thereby activating clock genes that promote the production of metabolites by various organs, including leptin, insulin, and ghrelin.[9]

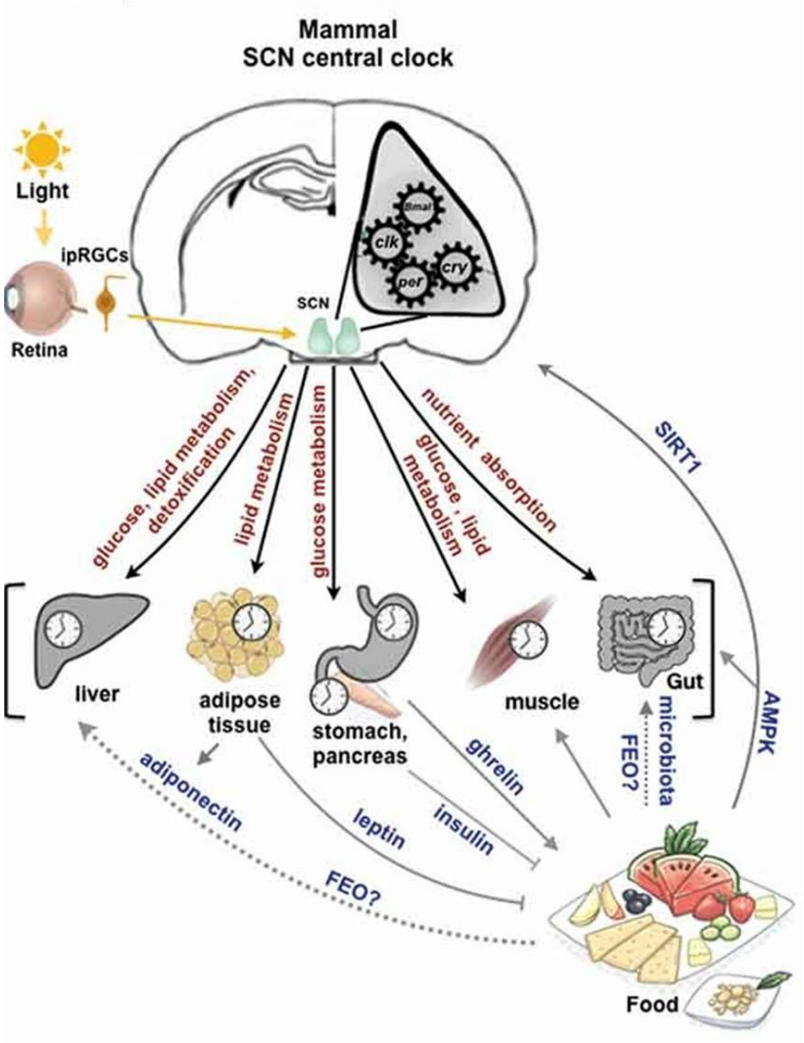

Figure 3: Square brackets collectively represent all the metabolic peripheral clocks, and blunt end lines represent inhibitory effects. Solid and dashed arrows represent known and putative pathways, respectively, involved in the interaction between clock and metabolism.[9]

A recent analysis of the circadian transcriptome and metabolome in cultured cells revealed that a substantial fraction—up to 28%—of all quantified metabolites exhibit rhythmicity. These metabolites are regulated by the biological clock in a cell type–specific manner and include amino acids as well as biosynthetic intermediates and precursors of NAD.[8]

The circadian clock regulates cellular metabolism through transcriptional control, imposing rhythmic expression on genes encoding metabolic enzymes involved in various pathways. Specifically, BMAL1 directly regulates genes encoding rate-limiting enzymes of several metabolic routes, such as phosphoenolpyruvate

carboxykinase (PEPCK) in gluconeogenesis, elongation of long-chain fatty acids protein 6 (Elovl6) in fatty acid biosynthesis, and triacylglycerol hydrolase in triglyceride breakdown.

In addition, clock proteins regulate the rhythmic expression and activity of other transcription factors, thereby imposing a circadian rhythm on their function. For instance, the transcription factors DBP, TEF, and HLF are under the control of the CLOCK–BMAL1 complex.

REV-ERBα regulates transcription both by directly binding to DNA, such as in the repression of core clock genes, and indirectly, through interactions with other transcription factors, as observed in the regulation of lipid metabolism genes. Moreover, REV-ERBα modulates the circadian transcription of Insig2 (Insulin-induced gene 2 protein), which encodes a transmembrane protein that sequesters SREBP proteins in the endoplasmic reticulum, thereby regulating their activity in cholesterol and lipid metabolism.

PER2, on the other hand, directly interacts with PPARα (Peroxisome proliferator-activated receptor alpha) to rhythmically modulate its target gene G6pc, which encodes glucose-6-phosphatase. PER2 also prevents the recruitment of PPARγ to promoters involved in lipogenesis, thus inhibiting lipid synthesis.

Studies on the circadian organization of metabolism have been primarily advanced using animal models with genetic disruption of circadian clock components. These studies have revealed the profound regulation of cellular metabolism by the circadian clock. This connection is reflected at the systemic level, where rhythmic cycles of metabolic processes manifest as oscillations in circulating and tissue metabolites.[2]

1.3 Circadian rhythms and mitochondria

Mitochondria are essential organelles and the powerhouses of eukaryotic cells; however, beyond their fundamental role in ATP generation though the process of oxidative phosphorylation. The acetyl groups are then introduced into the Krebs cycle, generating high-energy electrons that are transferred along the mitochondrial respiratory chain. This electron transfer drives proton flux across the inner mitochondrial membrane, ultimately enabling ATP synthesis by the ATP synthase complex.[10]

Through this intricate series of biochemical reactions, mitochondria convert metabolic fuels into the universal energy currency of the cell, ensuring that tissues meet their varying energetic demands.

Moreover, they are also involved in essential cellular processes such as lipid degradation, calcium homeostasis, and apoptosis. Given their central role in growth and homeostasis, mitochondrial dysfunction is associated with severe pathologies, including myopathies, neuropathies, and cardiovascular disorders.

In recent years, in addition to the various aspects of circadian regulation of cellular metabolism, increasing attention has been directed toward the circadian control of mitochondrial function. Indeed, growing evidence supports the existence of daily rhythms in mitochondrial content, dynamics, and functional activities, including respiration and ATP production, thereby indicating a widespread interaction between the circadian clock and organelle metabolism.[8]

1.3.1 Mitochondria, NAD^+ and clock genes

The molecule involved in a wide range of cellular mechanisms and linking metabolism, mitochondrial function, and circadian rhythms is Nicotinamide adenine dinucleotide (NAD^+).

NAD+ is an essential redox coenzyme that exists between the oxidized form NAD+ and its reduced form (NADH). NAD+ and NADH ratios are particularly important for processes including energy generation, metabolic

homeostasis, mitochondrial function, and DNA repair. NAD+ levels are tightly controlled in terms of production and consumption to ensure maintenance of cellular health.[11]

NAD^+ plays a central role in numerous metabolic pathways, including glucose catabolism during glycolysis, where it contributes to ATP production. It is also essential for fatty acid metabolism through β-oxidation, for glutaminolysis leading to the generation of α-ketoglutarate, and for the mitochondrial shuttling of metabolites.

Beyond its function as a redox cofactor, NAD^+ serves as a donor of ADP-ribose for enzymes such as poly (ADP-ribose) polymerases (PARPs), which are involved in DNA repair. NAD^+ also acts as a precursor of cyclic ADP-ribose (cADPR), a secondary signaling molecule generated by specific enzymes. Moreover, it can be hydrolyzed by sirtuins, NAD^+-dependent deacetylases that modulate histone acetylation and regulate gene expression.[11]

Synthesis of the complete NAD+ molecule is achieved via different biochemical pathways, namely the de novo synthesis, Preiss–Handler, salvage pathway, and the nicotinamide riboside kinase (NRK)-mediated salvage.

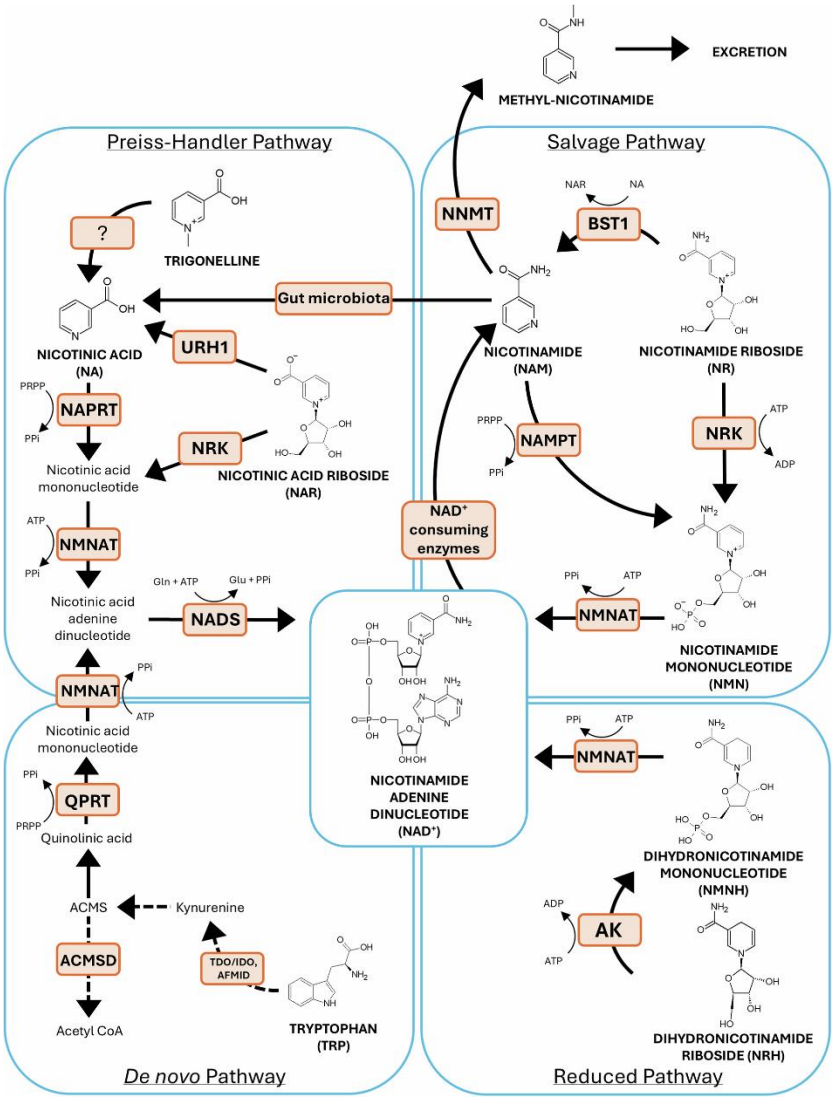

Figure 4: Different biochemical routes for NAD^+ formation. NAD^+ can be synthesized de novo from tryptophan (Trp), which merges with the Preiss–Handler pathway, which also uses nicotinic acid (NA) for the processing of deamidated precursors. The salvage pathway utilizes amidated precursors and allows recycling of the nicotinamide (NAM) byproduct of NAD^+-consuming enzymes. Reduced NMN (NMNH) and NR (NRH) are proposed to proceed through NADH to generate NAD^+.[11]

NAD^+ is predominantly concentrated in the mitochondria, with comparatively lower levels in the nucleus and cytoplasm. Within mitochondria, NAD^+ is essential for key metabolic processes, including the tricarboxylic acid (TCA) cycle, fatty acid β-oxidation, and oxidative phosphorylation (OxPhos).

Beyond its direct role as a substrate for the TCA cycle and the electron transport chain, much of NAD^+'s influence on mitochondrial homeostasis is

mediated through NAD^+-dependent enzymes, particularly the sirtuins. Mitochondrial sirtuin 3 (SIRT3) serves as a central regulator of mitochondrial metabolism, overseeing processes such as the mitochondrial unfolded protein response (UPR^{mt}), mitochondrial biogenesis, mitophagy, dynamics (fusion and fission), and the expression of antioxidant enzymes. In the nucleus, SIRT1 deacetylates and activates peroxisome proliferator-activated receptor gamma coactivator 1-alpha (PGC-1α), which in turn promotes mitochondrial biogenesis and enhances overall mitochondrial function.[11]

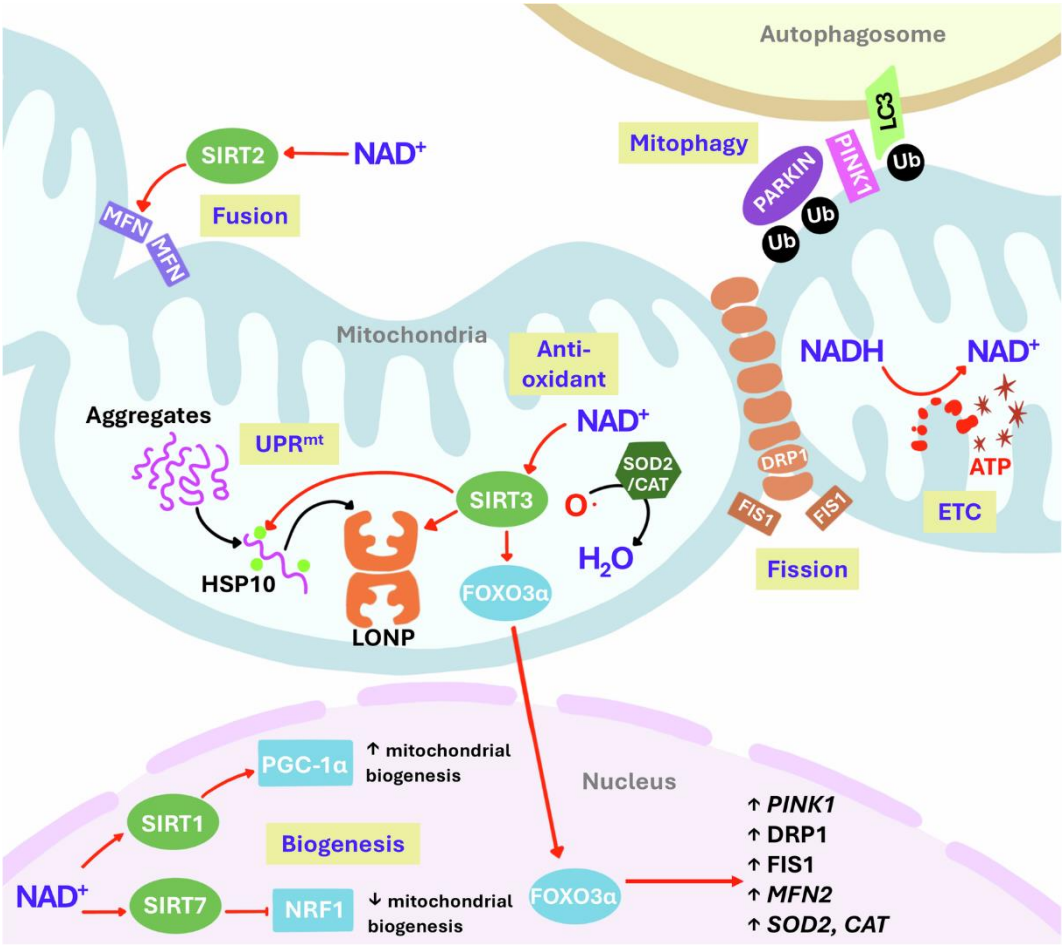

Figure 5: Different contributions of NAD^+ to mitochondrial homeostasis.

Among the NAD^+ biosynthesis processes, two molecules are considered key enzymes: Nicotinamide Mononucleotide Adenylyltransferase (NMNAT) and nicotinamide phosphoribosyltransferase (NAMPT).

NMNAT is considered a key enzyme in NAD^+ biosynthesis. Moreover, it plays a critical role in regulating mitochondrial homeostasis, genome stability, neuroprotection, healthy aging, and longevity.[12]

The circadian clock regulates the NAD^+ pathway by imposing rhythmicity NAMPT, the enzyme catalyzing the rate-limiting step in NAD^+ synthesis. The canonical role of NAD^+ is to facilitate hydrogen transfer in metabolic pathways.[13] NAD^+ is converted to NADH in four steps of the tricarboxylic acid (TCA) cycle, during which acetyl-CoA is oxidized to carbon dioxide. NAD^+ is also reduced to NADH during fatty acid and amino acid oxidation within mitochondria. In these mitochondrial pathways, the NADH generated serves as an electron donor for oxidative phosphorylation and ATP synthesis.

Beyond these canonical roles, poly (ADP-ribose) polymerases (PARPs) transfer ADP-ribose from NAD^+ to themselves, histones, and other proteins at sites of DNA damage, facilitating repair and maintaining genomic integrity. Damaged DNA recruits PARPs, activating their in-situ poly-ADP-ribosylation. Acute DNA damage, for instance caused by ionizing radiation, can thus trigger a rapid depletion of NAD^+ due to PARP activation. NAD^+ synthesis is regulated by the circadian machinery, providing a direct link between the circadian clock and metabolic pathways.[12]

The “clock genes” that impose rate-limiting control on NAD^+ biosynthesis are BMAL1 and CLOCK, which act on NAMPT.[14] Consequently, NAD^+ is systematically synthesized in a circadian oscillatory manner, creating a circadian program for sirtuin activation and mitochondrial metabolism.[14]

SIRT1, for example, can be regulated by multiple mechanisms, including transcriptional and post-translational modifications, changes in protein stability, phosphorylation, SIRT1-binding proteins, and fluctuations in NAD^+ levels.[14] The cytoplasmic and nuclear enzyme SIRT1, a member of the sirtuin family, is therefore activated in response to changes in NAD^+ concentration. SIRT1 rhythmically deacetylates BMAL1, deacetylates PER2 to reduce its activity, and regulates PGC-1α activity. There also appears to

be an indirect regulation of redox metabolism by the circadian clock through the NAMPT–NAD^+–SIRT3 axis.[13]

1.3.2 Mitochondrial DNA and circadian rhythm

The main and the most important activity of mitochondria is oxidative phosphorylation (OXPHOS). It is responsible for producing the vast majority of the cell's ATP, the primary energy currency that fuels most biological reactions.

Mitochondria have their own DNA known as mitochondrial DNA (mtDNA). The human mitochondrial genome itself is a compact, double-stranded, circular DNA molecule present in multiple copies within each cell. Unlike nuclear DNA, which generally exists in just two copies per cell, mtDNA is highly abundant: a typical human cell carries anywhere from several hundred to several thousand copies.

In mammals, every protein encoded by mtDNA contributes directly to the structure or function of the OXPHOS apparatus. Although the OXPHOS system is composed of around 90 individual protein components, mtDNA encodes 13 of them, all of which are essential for the proper operation of the respiratory chain.[15]

Human mtDNA is a 16 569 bp circular dsDNA molecule with genes encoded on both strands. In addition to encoding protein products of the OXPHOS machinery, mtDNA also encodes all of the RNA molecules required for the expression of these proteins, consisting of a minimal set of 22 tRNAs and two ribosomal RNAs.[15]

The mtDNA is independent of the nuclear DNA and possesses an independent replication, transcription, and translation machinery. Mitochondrial is a maternal inheritance.[16]

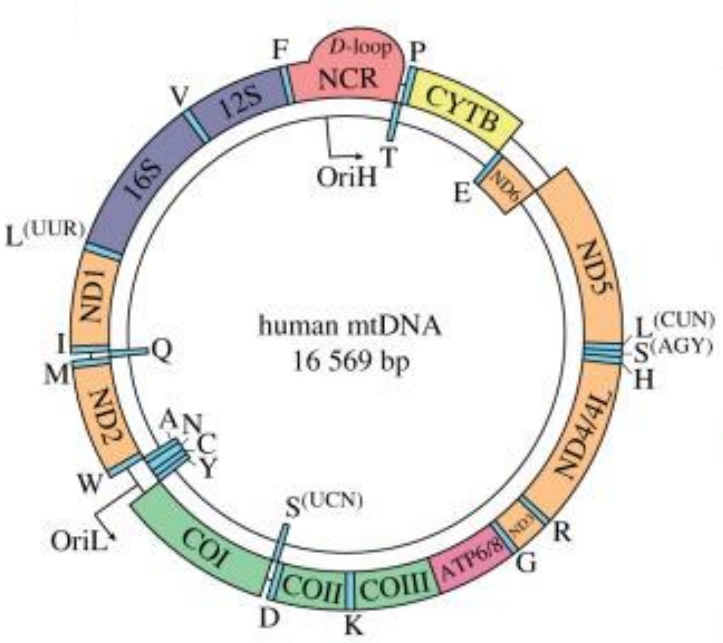

Figure 6: Map of human mitochondrial DNA (mtDNA). The loci of genes encoded on the L-strand (inner circle) and the H-strand (outer circle) are indicated.[15]

Another topic that has gained attention in recent research on mitochondrial DNA is its involvement in the molecular mechanisms governing cellular timing, as well as the extent to which these processes are influenced by circadian rhythmicity.

Research on mouse skeletal muscle identified that AMPK, a serine-threonine kinase, directly phosphorylates PGC1-α at Thr-177 and Ser-538, enhancing its transcriptional activity by inducing its promoter, thereby stimulating mitochondrial biogenesis via Transcription Factor A, Mitochondrial (TFAM), encoded by the nuclear DNA as a precursor. After expression, TFAM is transported to the mitochondrial matrix by the encoded Mitochondrial targeting signal peptides and the mitochondrial import machinery.[16]

TFAM is responsible for mtDNA replication and transcription, regulated by Ca2+ levels, and post-translational modifications such as acetylation at Lys-76 by acetyltransferase GCN5L1 and phosphorylation at Ser-55 and Ser-56 by protein kinase A and Ser-177 by extracellular signal-regulated kinase 1/2 (ERK1/2) on TFAM. Transcribed mtDNA is translated by mitochondrial

initiation factors such as mtIF2 and mtIF3, Elongation factors: EFTU, EF-TS, and mtEF-G1, Release factor (MTRF1L), Ribosome recycling factors such as MRRF and EF-G2mt, and Mito ribosomes.

Figures 7 and 8 depict the various upstream and downstream pathways of TFAM, which may, in turn, be modulated by circadian clock genes.

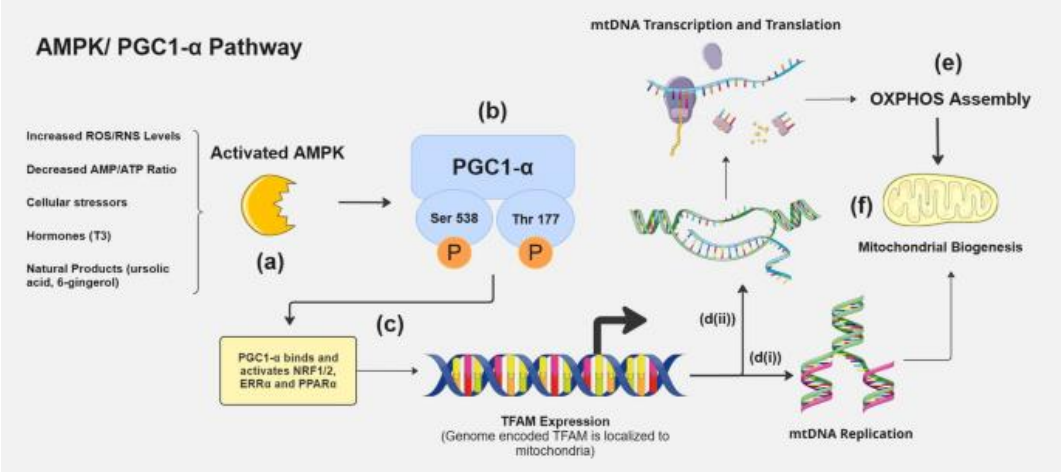

Figure 7: An overview of the AMPK/PGC1-α pathway. The figure highlights (a) AMPK activation induced by environmental and intracellular stressors via upstream serine/threonine kinases- Liver Kinase B1 (LKB1) and Calcium/Calmodulin-dependent protein kinase kinase beta (CAMKKβ), (b) PGC1-α phosphorylation by active AMPK at Ser-538 and Thr-177, (c) NRF1/2, ERRα, and PPARα activation and subsequent TFAM expression and regulation of (d(i)) mtDNA replication and (d(ii)) transcription, (e) OXPHOS complex assemblage and (f) mitochondrial biogenesis.[16]

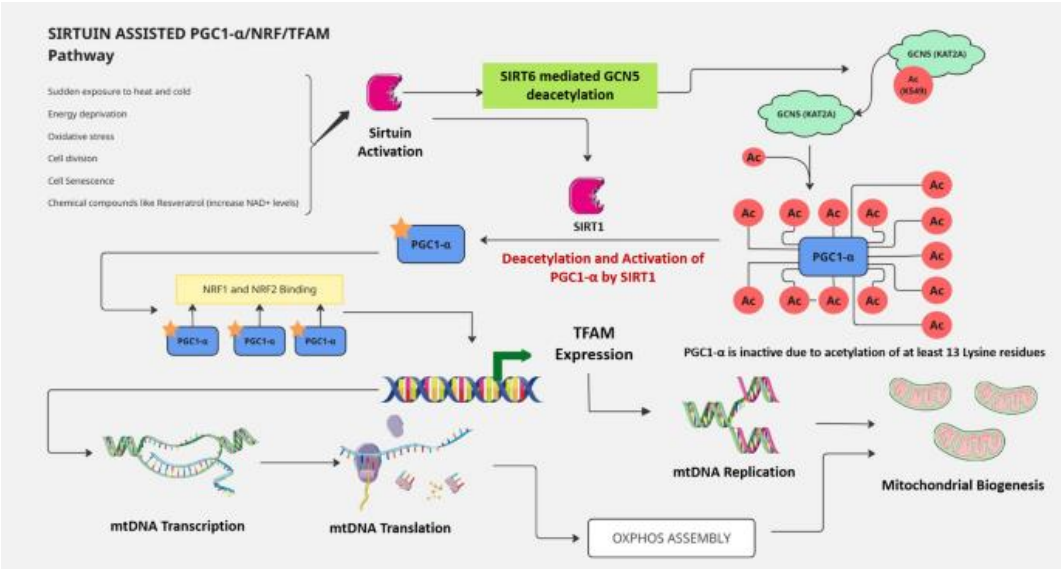

Figure 8: An overview of the Sirtuin Assisted PGC1-α/NRF/TFAM pathway. The figure depicts the following steps: (i) Sirtuin activation is triggered by external stressors and

cellular function, (ii) SIRT6 (Silent information regulator 6) mediates deacetylation of GCN5 at its Lys 549 residue, (iii) deacetylated GCN5 mediates poly-acetylation and subsequent inactivation of PGC1-α, and subsequent hepatic gluconeogenesis suppression, (iv) SIRT1 mediates deacetylation and activation of PGC1-α when the cell experiences stress-externally or internally, (v) PGC1-α binds to NRF1/2 and (vi) subsequently TFAM is transcriptionally activated, for regulating mitochondrial biogenesis. SIRT6 mediated PGC1-α inactivation usually occurs during (a) times when the cell does not experience stress, especially during the dark phase of the circadian rhythm, and (b) as part of a feedback mechanism to keep mitochondrial biogenesis in check and prevent disruption of the energy homeostasis.[16]

The direct circadian influence of mitochondrial initiation and elongation factors is currently being researched, their impact on mitochondrial protein synthesis and the assembly and stability of the OXPHOS assembly would, in turn, significantly affect circadian function. This is because the OXPHOS assembly, made up of 13 polypeptide subunits encoded by the mtDNA, and several nuclear-encoded mitochondrial proteins, generates ATP, which fuels all cellular processes, including the circadian rhythm, and regulates the expression of core clock genes as a non-light-based zeitgeber, exhibiting a 24-hour periodicity, and circadian oscillation.

Cell-free mitochondrial DNA (cf-mtDNA) is also regulated by circadian clock genes. Cf-mtDNA functions as a Damage-Associated Molecular Pattern (DAMP) and is closely linked to cytokine release, inflammation, and immune responses. The critical role of BMAL1 in cf-mtDNA–mediated inflammatory responses under hypoxia-induced injury, such as acute mountain sickness (AMS), has been demonstrated using smooth muscle cells from Bmal1 knockout mice. Bmal1 deletion significantly reduced mtDNA leakage, lowering cf-mtDNA levels and inflammation, highlighting the circadian regulation of cf-mtDNA–mediated immune responses.

Cf-mtDNA can also be transported between cells via extracellular vesicles (EVs). Encapsulated within EVs, cf-mtDNA (EV mtDNA) is shuttled to other cells, contributing to systemic inflammation. Higher circulating levels of EV-encapsulated cf-mtDNA have been observed in frail, middle-aged individuals, emphasizing its role in “inflammaging,” a form of chronic, low-grade inflammation linked to aging and age-related disorders such as frailty, osteoarthritis, Alzheimer’s and Parkinson’s diseases, cardiovascular diseases, and cancer.

Downregulation of BMAL1 may help reduce mtDNA leakage, thereby preventing both localized and systemic inflammatory responses.[16]

1.3.3 Circadian control of mitochondria respiration

Mitochondrial respiratory capacity to be synchronized with the light-dark cycle, ensuring optimal energy utilization at the appropriate time of day. The regulation of mitochondrial processes by the circadian clock, however, is complex, since external rhythmic factors. To isolate the specific contribution of the biological clock, researchers use a variety of experimental approaches, including genetic disruption of key transcriptional–translational feedback loop (TTFL) components such as Bmal1, Clock, Per2, and Cry1. In rodent models, these manipulations allow investigators to study how a dysfunctional clock impacts mitochondrial physiology. Other methods include time-restricted feeding paradigms that separate the effects of nutrient timing from circadian control, or the maintenance of animals under constant dark and fasting conditions to eliminate acute external stimuli. Complementary in vitro models, such as synchronized cell cultures treated with serum shock, permit investigation of clock-driven mitochondrial mechanisms without behavioral or systemic confounders, though these systems lack the full complexity of organ-level regulation.[17]

Further evidence that mitochondrial function is regulated by clock genes comes from studies on synchronized muscle cells in culture, which display cyclic changes in OCR over an approximate 24-hour period. Moreover, mitochondria isolated from mice exhibit time-of-day–dependent differences in nutrient utilization. In the presence of certain fatty acids, mitochondria show rhythmic respiration, peaking around the transition from the active to the rest phase; this pattern is driven by the synchronous rhythmicity of carnitine palmitoyl-transferase 1 (CPT1), the rate-limiting enzyme for mitochondrial fatty acid uptake. Similarly, pyruvate utilization appears to be rhythmic, likely due to circadian cycles of phosphorylation and dephosphorylation of pyruvate dehydrogenase (PDH).[8]

Disruption of clock genes such as Per1/2 abolishes these rhythmic patterns, indicating that the PERIOD proteins play a critical role in aligning mitochondrial fuel usage with daily energy requirements.

Experimental analyses using both cell culture and animal models provide compelling evidence for rhythmic mitochondrial respiration.

The oxygen consumption rate (OCR), a key indicator of mitochondrial respiratory activity, exhibits 24-hour oscillation.

At the hepatic level, a large portion of the transcriptome, proteome, and metabolome exhibits tissue-specific circadian rhythmicity and has been extensively studied in both cellular and animal models. In a 2016 study by Scrima et al., it was shown that inhibition of Bmal1 transcription via siRNA in a liver-derived cell line (HepG2) led to a decrease in mitochondrial respiration. To further investigate this, HepG2 cells were synchronized using a serum shock, and it was observed that following synchronization, the cells displayed rhythmic respiratory activity, peaking at synchronization time (ST) 12 hours, corresponding to the first zenith.[18]

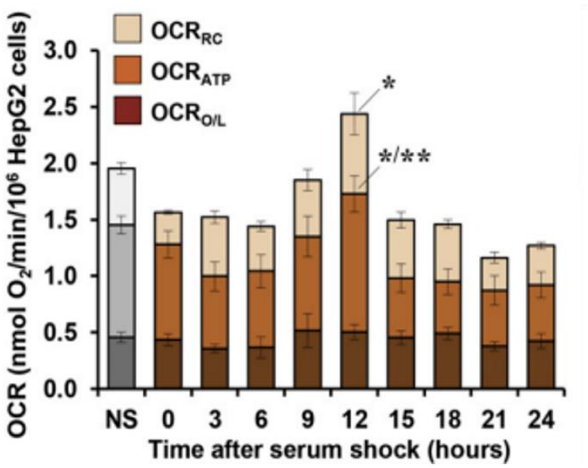

Figure 9: Measurement of mitochondrial respiratory activity in intact cells. In the histogram, the overlaid bars represent the oxygen consumption rate (OCR), with the subscripts "O/L," "ATP," and "RC" referring to oligomycin-controlled proton leak respiration, ATP synthase-dependent respiration, and reserve respiratory capacity, respectively; "NS" denotes non-synchronized cells.[18]

In these synchronized cells, the expression levels of ARNTL/BMAL1 were also analyzed. It was found that the oscillatory profile of both transcripts

and proteins mirrored the dynamics observed in the cellular respiration profile. Specifically, the peak expression of BMAL1 mRNA and protein preceded that of respiratory activity by approximately 3 hours.

In parallel, the transcription of the NR1D1 gene, which encodes REV-ERBα and functions as a negative regulator of BMAL1, was assessed. The oscillatory profile of NR1D1 was almost opposite to that of BMAL1, with a delay of approximately 6 hours relative to the peak expression of BMAL1.[18]

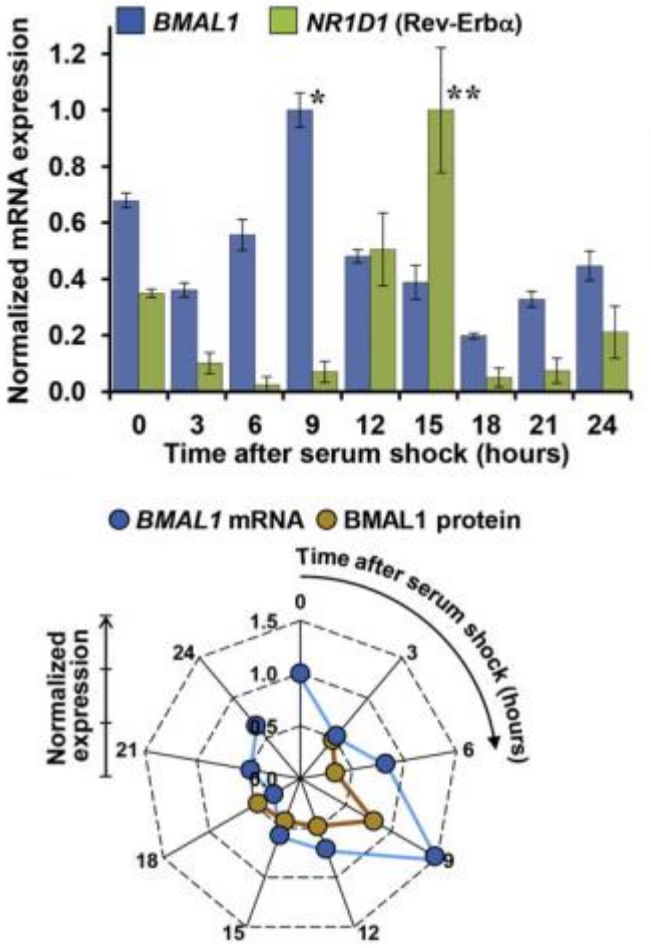

Figure 10: Expression of BMAL1 and NR1D1. The upper histogram depicts the transcriptional levels of BMAL1 and NR1D1 (REV-ERBα) as determined by qRT-PCR. Values, normalized to their respective peaks, are presented as means ± S.E.M. from n = 3–4 independent experiments, each including three technical replicates. The lower circular diagram illustrates a comparison between BMAL1 mRNA expression and protein levels, measured by qRT-PCR and densitometric analysis of immunoblots, respectively. Values, normalized to ST = 0, represent n = 3 independent experiments (technical replicates excluded).[18]

HepG2 cells in which BMAL1 expression was suppressed by RNA interference exhibited a markedly abrogated oscillation of OCR.

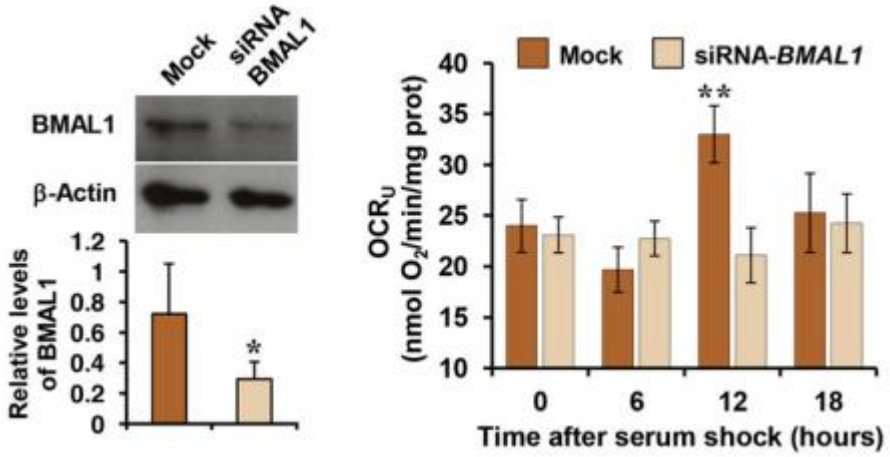

Figure 11: Effect of BMAL1 silencing on OCR. On the left, a representative immunoblot of BMAL1 in HepG2 cells transfected with siRNA targeting BMAL1, with densitometric analysis normalized to β-actin. The histogram on the right depicts uncoupled OCR in synchronized cells.[18]

These results, together with additional evidence, suggest that in vitro, synchronized cells exhibit an autonomous ultradian oscillation of mitochondrial OXPHOS activity, which is linked to the expression of core clock genes.

To investigate this further, OCR was measured in both whole cells and isolated mitochondria to assess nutrient utilization and mitochondrial respiration in wild-type mice versus mice lacking specific clock genes. Notably, mitochondria isolated from the livers of Bmal1 knockout mice, liver-specific Bmal1 knockouts, and Per1/Per2 double knockouts displayed lower OCRs compared to their corresponding wild-type controls.[18]

Mitochondria isolated from various tissues, including liver, muscle, and brain, show similar dependencies: wild-type mitochondria exhibit higher OCR and FAO activities than those derived from Bmal1 or Per1/2 knockout animals.[10] Measurements using radiolabeled fatty acids confirm that FAO rates are diminished in Bmal1-deficient mice, reinforcing the notion that the molecular clock is a key determinant of mitochondrial substrate oxidation.

Interestingly, the temporal patterns of mitochondrial respiration differ depending on the supplied substrate. In the presence of succinate,

respiration remains relatively constant throughout the day, whereas supplementation with fatty acid oxidation substrates such as palmitoyl-carnitine or palmitoyl-CoA plus carnitine produces rhythmic respiration that peaks early in the light phase, coinciding with elevated CPT1 protein levels. In contrast, carbohydrate-derived substrates like pyruvate and malate support respiration that peaks later in the light phase, indicating that mitochondrial substrate preference shifts over the circadian cycle. Differences observed between isolated mitochondria and intact hepatocytes suggest that extrinsic cellular factors also modulate mitochondrial rhythms beyond the intrinsic clock machinery. Importantly, these daily variations are further influenced by environmental and behavioral factors such as nutrient type, dietary composition, and feeding pattern (e.g., night-time restricted feeding or high-fat diet). Collectively, these findings demonstrate that mitochondrial respiration and nutrient utilization follow robust daily oscillations shaped by the interplay between the molecular circadian clock, metabolic substrates, and systemic physiological cues.[10]

1.3.4 Mitochondrial biogenesis and circadian clock

Mitochondrial biogenesis is a complex and highly regulated process composed of two closely interconnected phases: proliferation, which increases the number of mitochondria per cell, and differentiation, which allows these organelles to acquire the structural and functional characteristics required for their specific cellular roles.[20]

This process depends on the precise coordination between the nuclear and mitochondrial genomes. The expression and replication of the mitochondrial genome must be synchronized with the transcription and translation of nuclear-encoded mitochondrial proteins, as well as with their import into the organelle. Protein import is mediated by the TOM and TIM complexes located in the outer and inner mitochondrial membranes, respectively. Several key regulators govern this communication between the two genomes, including nuclear respiratory factors 1 and 2 (NRF1, NRF2), mitochondrial transcription factor A (TFAM), and the peroxisome

proliferator-activated receptor gamma coactivator 1-alpha (PGC1α). Among these, PGC1α plays a central role as a coactivator that enhances the activity of transcription factors such as NRF1 and NRF2, thereby promoting the transcription of nuclear genes encoding mitochondrial proteins. Through this coordinated regulation, PGC1α simultaneously controls the expression of both nuclear and mitochondrial genes involved in mitochondrial biogenesis and oxidative metabolism, maintaining lipid, glucose, and energy homeostasis.[19]

Mitochondrial content, which reflects the outcome of mitochondrial biogenesis, is typically assessed through measurements of mitochondrial DNA (mtDNA) copy number and mitochondrial protein levels. Although PGC1α is rhythmically expressed in mouse liver and skeletal muscle as well as in synchronized HepG2 cells, there remains considerable debate as to whether mitochondrial content itself exhibits a circadian rhythm.[21] reported 24-hour oscillations in mtDNA copy number and mitochondrial protein content, detected using MitoTracker, that were dependent on the circadian gene Bmal1. In contrast, other studies found no rhythmicity in mtDNA copy number or in protein levels of respiratory chain complexes and the outer membrane protein Tomm20. Furthermore, discrepancies between mitochondrial content and mtDNA copy number have been observed in models deficient in circadian clock genes. In particular, Bmal1 deficiency leads to reduced PGC1α expression and decreased mitochondrial protein content, while mtDNA copy number fails to accurately reflect these changes, indicating that mtDNA alone is an unreliable marker of mitochondrial abundance.[22]

Further evidence for the circadian regulation of mitochondrial biogenesis comes from studies in rodent knockout models. In mouse embryonic fibroblasts lacking Per2, mitochondrial number and mtDNA copy number remain unchanged, suggesting that not all components of the circadian machinery directly influence mitochondrial abundance. However, in Per1/2 double knockout mice, daily oscillations of key mitochondrial enzymes such as CPT1 and PDH, as well as proteins involved in oxidative phosphorylation, are abolished. Moreover, the average protein content of PDH is reduced,

implying that PER proteins contribute to the regulation of mitochondrial protein synthesis and possibly biogenesis itself. In contrast, liver-specific Bmal1 knockout mice show no alteration in overall mitochondrial content or in Pgc1a mRNA and protein levels, although Pgc1b expression loses rhythmicity and decreases under global Clock mutation or Bmal1 deficiency. Collectively, these findings indicate that PGC1α, rather than PGC1β, serves as the primary regulator of the circadian rhythm of mitochondrial biogenesis. Disruption of PGC1α impairs mitochondrial abundance, alters mitochondrial volume, and reduces protein content, confirming its central regulatory role.

Importantly, the transcription of Pgc1a does not appear to be driven by the positive limb of the circadian transcription–translation feedback loop (TTFL), but interference with the negative limb reduces PGC1α protein expression and mitochondrial content. The molecular connection between the TTFL and PGC1α activity is thought to involve nutrient-sensing pathways mediated by AMPK and SIRT1. Indeed, it has been shown that REV-ERBα can enhance PGC1α activity through AMPK-dependent activation of SIRT1, establishing a direct link between cellular metabolic state and circadian control of mitochondrial biogenesis.[22]

1.3.5 Mitochondrial dynamics and circadian clock

Mitochondria possess a double-membrane structure that defines their unique organization within the cell. The outer mitochondrial membrane (OMM) faces the cytosol, while the inner mitochondrial membrane (IMM) folds inward into the mitochondrial matrix, which contains the mitochondrial DNA (mtDNA). The compartment enclosed between the IMM and the OMM is known as the intermembrane space (IMS).

Mitochondria are highly dynamic organelles capable of remodeling their morphology to form an interconnected tubular network through coordinated cycles of fission and fusion. The balance between these opposing processes, collectively referred to as mitochondrial dynamics,

determines the number, size, and spatial distribution of mitochondria within the cytoplasm.

These dynamic transitions are fundamental not only for maintaining mitochondrial functionality but also for enabling the organelle to adapt its morphology to cellular energy requirements, nutrient availability, and the metabolic status of the cell. Moreover, different mitochondrial morphologies are strongly associated with a wide range of physiological and pathological conditions.

Mitochondrial fission involves the division of a single mitochondrion into two daughter organelles, whereas mitochondrial fusion refers to the merging of two mitochondria into one continuous structure. Disruption of the precise regulation of these spatial and temporal processes results in distinct morphological outcomes: either a fragmented network composed of numerous small, spherical mitochondria, or a hyperfused network with elongated, highly interconnected structures.

The main proteins composing the core machinery are large GTPase proteins belonging to the Dynamin family. These mechanoenzymes can oligomerize and change conformation to drive membrane remodeling, constriction, scission, and/or fusion. Mitochondrial fission is carried out by the Dynamin-related/-like protein 1 (DRP1) and Fis1, and MFF (Mitochondrial Fission factor). Mitochondrial fusion is ensured by mitofusins 1 and 2 (MFN1 and MFN2) and optic atrophy 1 (OPA1), with the accessory proteins Misato (MSTO1) and FBXL4 which mediate OMM and IMM fusion, respectively.[23]

MFN1 and MFN2, located on the OMM, mediate membrane tethering and fusion. MFN1 exhibits stronger GTPase and tethering activity, serving as the main driver of mitochondrial outer membrane fusion, whereas MFN2 participates in later stages. Their activity is fine-tuned by post-translational modifications, including acetylation and ubiquitination. MSTO1 supports fusion by interacting with mitofusins at the OMM, while FBXL4 forms multiprotein complexes that may regulate fusion dynamics.

OPA1, anchored to the IMM, governs inner membrane fusion and cristae remodeling. Its activity depends on membrane potential: long OPA1

isoforms promote fusion, whereas stress-induced cleavage by OMA1 generates short isoforms that inhibit fusion, a process counterbalanced by the protease YME1L1.[23,24]

Deficiency in functional circadian clock components leads to abnormal mitochondrial morphological dynamics and consequent mitochondrial dysfunction. In liver-specific Bmal1 knockout mice, mitochondria appear enlarged and swollen throughout the day, a phenotype associated with reduced expression of mitochondrial fission proteins. In contrast, CLOCKΔ19 mice display smaller and more fragmented mitochondria, along with a loss of rhythmic changes in mitochondrial morphology. This disruption results in impaired mitochondrial homeostasis, characterized by reduced respiration rates, lower ATP levels, and increased production of reactive oxygen species (ROS).

Moreover, ChIP-sequencing analyses have demonstrated that the circadian regulators Bmal1, Clock, and Cry1 bind to the promoters of several mitochondria-related genes, including *Fis1*, *Bnip3*, and *Pink1*. Recent studies have identified Drp1 as a key molecule linking circadian regulation of mitochondrial morphology with cellular bioenergetics. The stability of *Drp1* mRNA is controlled by CLOCK through its interaction with the RNA-binding protein PUF60.

Suppression of Drp1 eliminates the rhythmic oscillations of both mitochondrial morphology and ATP levels, underscoring its significant role in the circadian regulation of mitochondrial architecture and function. In liver-specific Bmal1 knockout mice, the expression of fission proteins (*Drp1*, *Fis1*) and mitophagy-related proteins (*Bnip3*, *Pink1*) is markedly reduced, and their rhythmic expression patterns are abolished.[25]

The morphological dynamics of mitochondria coincide with oscillations in ATP content and OXPHOS activity: Mitochondrial fusion induces a tubular network, resulting in an increase in ATP content and high OXPHOS activity, while fragmented forms induced by mitochondrial fission lead to the opposite results.[25]

1.3.6 Mitophagy and circadian clock

Mitochondrial clearance is accomplished through a specialized form of autophagy called mitophagy, which selectively targets damaged or dysfunctional mitochondria for degradation. Circadian regulation of autophagy is supported by evidence showing that the number of autophagic vacuoles varies throughout the day across multiple tissue types, highlighting the temporal coordination of mitochondrial turnover with the molecular clock.[17]

Mitophagy serves as a key quality control mechanism to prevent the accumulation of defective mitochondria, which could otherwise lead to excessive production of reactive oxygen species (ROS), cytotoxicity, and cellular aging. This process is particularly important under stress conditions, such as hypoxia, where mitophagy functions as an adaptive metabolic response to eliminate damaged mitochondria and reduce the risk of cell death. Mitochondrial turnover typically occurs on a timescale of approximately 15 days.[19]

At the molecular level, mitophagy is orchestrated primarily by the PTEN-induced kinase 1 (PINK1)/Parkin pathway. When mitochondria lose their membrane potential due to damage, PINK1 stabilizes on the outer mitochondrial membrane rather than being imported and degraded by the inner membrane protease PARL. Stabilized PINK1 then recruits the cytosolic E3 ubiquitin ligase Parkin, which ubiquitinates mitochondrial outer membrane proteins such as mitofusin-1 and mitofusin-2. These ubiquitinated proteins are recognized by adaptor proteins such as p62 and HDAC6, which bind to LC3, an adaptor protein that recruits selected mitochondria to autophagosomes, promoting their engulfment for further degradation. The active form of LC3 is the lipidated protein LC3-II, derived from the LC3-I precursor.

This selective targeting ensures that only damaged mitochondria are degraded, while healthy mitochondria are spared through PINK1 import and proteolytic degradation, which depends on maintaining membrane potential.[19]

Mitophagy is linked to circadian clock genes. Although Pgc1a levels fluctuate throughout the day, overall mitochondrial mass and content are generally stable under normal conditions. Disruption of the molecular clock, however, affects mitochondrial properties in both animal and human cellular models. In the liver of mice, mitochondrial biogenesis exhibits a clear diurnal rhythm that is Bmal1-dependent, as liver-specific Bmal1 knockout abolishes the rhythmic pattern of mitochondrial biogenesis.[21] This observation suggests that if mitochondrial biogenesis oscillates throughout the day while mitochondrial content remains largely unchanged, additional regulatory mechanisms, such as mitochondrial removal, must act as a counterbalance to maintain mitochondrial homeostasis.[17]

Following recruitment of Parkin, proteasomes are directed to the damaged mitochondria in a Parkin-dependent manner, degrading outer mitochondrial membrane proteins and potentially inducing mitochondrial fragmentation. Importantly, proteins within the inner membrane and matrix remain largely intact, preserving mitochondrial core functions while enabling removal of dysfunctional organelles. The bioenergetic status of mitochondria plays a critical role in regulating PINK1 stabilization and subsequent Parkin recruitment, ensuring that mitophagy is efficiently triggered only under conditions of mitochondrial impairment.[19]

Overall, the interplay between circadian-regulated mitochondrial biogenesis and selective mitophagy allows cells to maintain a stable mitochondrial population, remove damaged organelles efficiently, and preserve cellular energy homeostasis, highlighting the importance of temporal coordination in mitochondrial quality control.

2. AIMS

The objective of this thesis is to broaden the current understanding that mitochondrial respiration is regulated by the molecular circadian clockwork across multiple cellular contexts, including both primary and tumor-derived cell types, through quantitative assessment of oxygen consumption. Moreover, this work aims to substantiate the hypothesis that the autonomous rhythmic oscillation of respiratory activity represents an intrinsic cellular phenomenon that occurs irrespective of the synchronization protocol adopted and of the diverse methodological approaches employed to quantify mitochondrial oxygen consumption rates under conditions mimicking distinct metabolic stressors.

Furthermore, by employing a well-established *in vitro* cellular model of the circadian clock machinery, this thesis seeks to examine the expression of mitochondrial genes encoding subunits of the respiratory chain, alongside key components of mitochondrial dynamics, including biogenesis, mitophagy, fission, and fusion.

3. MATERIALS AND METHODS

3.1 Cell cultures

For this project all the cell types were purchased from ATCC (https://www.atcc.org).

All the cell types used in the present study were purchased from ATCC. Cell cultures were maintained in the DMEM-based specific medium, as reported by the manufacturer, at 37 ◦C in the presence of 5% CO2 supplemented with 10 mM HEPES, 10% inactivated fetal bovine serum (FBS), 2 mM glutamine, 100 U/mL of penicillin and 100µg/mL of streptomycin.

Cell types are:

- HAEC → Normal Primary Human Aortic Endothelial Cells
- NHDF → Normal Human Dermal Fibroblasts
- CAL 27 → Tongue epithelial cells, Squamous Cell Carcinoma
- SCC-9 → Tongue cell lines, Squamous Cell Carcinoma
- Hela → Cervix epithelial cell lines, Adenocarcinoma
- HepG2 → Liver cells lines, Hepatocellular carcinoma
- U-2 OS → Bone epithelial cell line, Osteosarcoma
- SW480 → Colon epithelial cell, Adenocarcinoma, Colorectal, Duke's type B
- SW620 → Colon epithelial cell, Adenocarcinoma, Colorectal, Duke's type C

3.2 In vitro Circadian Rhythms synchronization

To study circadian rhythms in vitro it is necessary to synchronize the transcription of clock genes. Serum shock deprivation method is used in this project. Cells are treated DMEM-based specific medium supplemented with 50% of Fetal Bovin Serum (FBS) for 2h and then medium is replaced by DMEM-based specific medium supplemented with 10 mM HEPES, 2 mM glutamine, 100 U/mL of penicillin and 100µg/mL of streptomycin.

Serum shock treatment activates directly the transcription of clock genes *PER1* and *PER2*.[26]

3.3 Bmal1 silencing in HepG2

BMAL1-specific siRNA was purchased from ThermoFisher (Mission Pre-designed siRNA). HepG2 cells were seeded on 60-mm dishes and at 30–50% confluence and transiently transfected with the BMAL1- specific siRNA and Scrambled siRNA (for negative control) diluted in Opti-MEM using Lipofectamine® 3000 Transfection Reagent (Invitrogen) according to the manufacturer's protocol. After 18–20h of incubation at 37 ◦ C, the transfection medium was replaced with complete medium containing 10% FBS and after 72h (where the maximal efficiency is reached) cells were collected and assayed.

3.4 Real-time PCR (qPCR)

The purification of total RNA from HepG2 cells was carried out by using Aurum Total RNA Mini Kit (Bio-Rad® Catalog # 732-6820 Hercules, California, USA) according to the manufacturer's protocol. 0.5μg of total RNA was then reverse-transcribed to generate cDNA for PCR by using the iScript cDNA Synthesis kit (Bio-Rad, Hercules, California, USA). Semi-quantitative determination of mRNA levels was performed by real-time PCR, using SYBR Green (Bio-Rad®, Hercules, California, USA). Reactions were performed in triplicate for each sample. Multiple reactions were performed in a volume of 20μl containing 10μl of 2× PCR master mix, 1× of validated specific primers (Qiagen, Venlo, The Netherlands), and cDNA template (50 ng). Amplifications were performed in the BIORAD Real- Time PCR Detection System CFX96 RT SYSTEM (Bio-Rad®, Hercules, California, USA), using the following cycle program: denaturation step at 95°C for 30s followed by 45 cycles of denaturation at 95°C for 10s, annealing at 60°C for

30 s, and extension at 65°C for 5 s. The relative mRNA expression levels were calculated by using the comparative CT method (Relative Quantification RT=2^-ΔΔct). Quantitative normalization for each sample was performed by using β-actin as an internal control. Validated primers were as follows: ND1, CYTB, COI, ATP6, β-actin (from BIORAD respectively qHsaCED0021828, qHsaCED0048354, qHsaCED0048374, qHsaCED0048397); NRF1, PGC1 α and TFAM (from QIAGEN respectively QT01154076, QT01006243 ,QT00012782) (Qiagen).

3.5 Electrophoresis and Western Blotting

Aliquots, containing 40μg of protein extracts from cell lysate. Protein extract was obtained with lysis buffer RIPA (50mM Tris HCl pH 8, 150mM NaCl, 1% Igepal, 0,5% Sodium Deoxycholate, 0,1% sodium dodecyl sulfate supplemented with protease inhibitor cocktail 1x). Protein samples were subjected to SDS-PAGE (10% acrylamide for separating gel and 4% for stacking gel) and transferred to a PVDF membrane (Bio-Rad® Laboratories, Hercules, CA, USA) using a Trans Blot Turbo Transfer System. Then membranes were probed with the following primary antibodies: anti-BMAL1 (rabbit polyclonal, Cell Signaling, D2L7G, dil. 1:1000); anti-COII (MTCO2) (mouse monoclonal, Invitrogen, 12C4F12, dil. 1:1000); anti-COIV (mouse monoclonal, Abcam, ab14744, dil. 1:1000); anti-ND1 (rabbit monoclonal, Abcam, ab181848, dil. 1:1000); anti-NDUFB8 (mouse monoclonal, Thermo Fisher, 20E9DH10C12, dil. 1:1000); anti- PGC1 α (rabbit polyclonal, Novus, NBP1-04676, dil. 1:1000); anti-LC3I/II (rabbit polyclonal, Cell Signaling, #4108, 1:1000); anti-MFN1 (rabbit polyclonal, Santacruz, sc-50330, dil. 1:1000); anti-MFN2 (rabbit monoclonal, Cell Signaling, #9482, dil. 1:1000); anti-OPA1 (mouse monoclonal, BD Transduction Laboratories, 612606, dil. 1:1000); anti-DRP1 (mouse monoclonal, BD Transduction Laboratories, 611112, dil. 1:1000); anti-β-actin (mouse monoclonal, A5441, Sigma, dil. 1:10,000). As secondary Abs

the following were used: HRP- conjugated anti-rabbit IgG (Thermo Scientific, dil. 1:10,000); and HRP-conjugated anti-mouse IgG (Bio-Rad®, 1:10,000). The signals were developed using the enhanced chemiluminescence kit (Clarity Western ECL Substrate, Bio-Rad), acquired with ChemiDoc imaging system XRS + (Bio-Rad®), and then analyzed using ImageLab software (Bio-Rad®).

3.6 Respirometric measurements

3.6.1 Clark electrode-based polarography

The oxygen consumption rates (OCRs) were measured in intact cells either by Clark electrode-based polarography or by an O2-sensitive fluorescent probe. For polarographic measurements, cultured cells were gently detached from the dish by trypsinization, washed in PBS, harvested by centrifugation at 500× g for 5 min and immediately assessed for O2 consumption with or Hansatech oximeter (Hansatech Instruments, Narborough Rd, Pentney, King's Lynn PE32 1JL, Regno Unito, UK). About 2–10 × 10^6 viable cells/mL were assayed in their specific culture medium at 37 ◦C; after attainment of a stationary endogenous substrate sustained basal oxygen consumption rate (basal OCR), 2 μg/mL of the ATP-synthase inhibitor oligomycin was added (leak OCR) followed by addition of 0.3μM of the uncoupler carbonilcyanide p-triflouromethoxyphenylhydrazone (FCCP) (maximal OCR). The rates of oxygen consumption were corrected for 2 μM antimycin A + 2μM rotenone-insensitive respiration and normalized to the initial cell number; the ATP-linked OCR was estimated from the difference between the basal OCR and leak OCR and the OCR reserve capacity from the difference between the maximal OCR and basal OCR.

3.6.2 Resipher system technology (Lucid Scientific Inc.)

Alternatively, the OCR was measured in real-time in adherent cells by Resipher system technology (Lucid Scientific Inc. Atlanta, GA, USA) following the manufacturer's protocol; 20,000 cells/100 μL/well were plated in the 96-well cartridge (in technical triplicates) and placed in the CO2 incubator at 37 ◦C with measurements of the basal OCR taken every 15 min for at least 36 consecutive hours; the first 3–4 h were not taken into account because of temperature equilibration.

3.6.3 Seahorse technology

For measurement of the metabolic fluxes, the Seahorse technology was used. Briefly, distinct groups of cell samples, plated in the multi-well cartridge, were subjected to the synchronization protocols following a 4 h out-of-phase time schedule enabling assessment of all the samples in the same experimental session. The OCR and extra-cellular acidification rate (ECAR) were measured simultaneously in adherent cells with a XF96 Extracellular Flux Analyzer (Seahorse Bioscience, Billerica, MA, USA). After replacing the growth medium with 180 μL of bicarbonate-free DMEM supplemented with 10 mM glucose 2 mM L-glutamine and 1 mM sodium pyruvate pre-warmed at 37 ◦C, cells were preincubated for 45 min before starting the assay procedure. After measuring the basal OCR and ECAR, oligomycin (1 μM), carbonyl cyanide m-chlorophenylhydrazone (0.5 μM), rotenone + antimycin A (1 μM + 1 μM) and 2-deoxy-glucose were injected into each well sequentially to assess the leak, maximal and non-mitochondrial OCR as described above. For the ECAR (an indirect estimate of glycolysis), addition of oligomycin caused an increase in the basal value and it is taken as a measure of the maximal glycolytic capacity (no significant changes were observed upon the successive addition of carbonyl cyanide m chlorophenylhydrazone androtenoneplusantimycinA);2-deoxy-glucose causedinhibition of the glycolytic flux and the residual ECAR was subtracted from the basal ECAR. The values were normalized to protein content in each well, determined with a BCA assay.

3.7 Confocal Microscopy analysis

HepG2 cells were cultured at low density on fibronectin-coated 35- mm glass-bottom dishes (Ibidi) and incubated for 20 min at 37 with 0.5 μM Mito Tracker Green and 3.6 μ M DAPI from Molecular Probes (Carlsband, CA, USA). Stained cells were washed with PBS and examined with Leica TCS SP8 confocal laser scanning microscopy system with fluorescence elicited with an Ar-Kr laser beam (λex 488nm). Mitochondria images were acquired by time-lapse, recording one image every 1h during 24 to 48 h. Each image is a stack of 10 scans over 20 acquisition, storage, and analysis of data both for HepG2 were performed with LasX software from Leica. Morphometric analysis of the mitochondrial network. Mitochondrial morphology was scored by software-based methods using ImageJ software and plugins. Images of both the Mito Tracker Green-stained HepG2 cells, and mitochondrial particles were analyzed for area (a), perimeter (p) and circularity (c). Metrics that reliably reported the morphology of the mitochondrial network are the cumulative area:perimeter ratio (Σa/Σp) and the elongation index ($1/c = p\ 2\ /\ (4\ \pi\ a)$). The cumulative area:perimeter ratio (or interconnectivity factor) is computed as the summed particle area in a region of interest divided by the summed particle perimeter (including the perimeter of enclosed spaces or “holes”). This metric is particularly effective at detecting the transition from elongated, isolated mitochondria to a reticular network of interconnected mitochondria. The elongation factor is reported as an average of all particles in a ROI, it has a minimum value of 1 (for perfect circles), and captures well the transition from punctiform to elongated, complex shaped, but still isolated mitochondria. About 50 single cells were analyzed for each imaging analysis for the “static” images with Mito Tracker Green-stained HepG2 cells, were analyzed for each frame in the time-lapse assay.

3.8 Cosinor analysis

The temporally resolved data measured in this study after in vitro synchronization were submitted to nonlinear regression analysis by the Cosinor equation: $f(t) = M + A\cos(2\pi t/P + \phi) + st$, where: t = time post synchronization; M = mesor (Midline Statistic Of Rhythm, a rhythm-adjusted mean); A = amplitude (a measure of half the extent of predictable variation within a cycle); P = period (duration of one cycle); ϕ = acrophase (a measure of the time of overall high values recurring in each cycle, corresponding at the time post-synchronization when the first peak appears); s = slope (gradual slant of the overall data-set pro f ile). The analyses were carried out with GraFit version 7 (Erithacus Software) by initial approximation of the parameters; several fitting routines/cycles were allowed till reaching a χ 2.7. Statistical analysis 2 <0.05.

4. RESULTS

4.1 Mitochondrial respiration undergoes autonomous oscillation in synchronized cells

In vitro–synchronized cells were analyzed to assess mitochondrial respiratory function by measuring the oxygen consumption rate (OCR). In most studies, OCR refers to the raw value, commonly termed basal OCR. This parameter reflects the oxidation of multiple substrates, including those intrinsic to the metabolic profile of the specific cell line and those provided by the culture or assay medium.

Basal OCR is sustained by the generation of an electrochemical proton gradient across the inner mitochondrial membrane, established through the proton-translocating activity driven by electron flow through respiratory chain complexes I, III, and IV. This protonmotive force supports several exergonic processes, most notably ATP synthesis, as well as the uptake of charged metabolites such as pyruvate and glutamate. The proton gradient can also be dissipated non-productively by passive proton leakage across the inner membrane or through the activity of uncoupling proteins.

As a result, basal OCR comprises two independently regulated components: an ATP-linked fraction and a proton leak–associated fraction. A widely used method to discriminate between these components involves measuring respiration in the presence of oligomycin, a specific inhibitor of ATP synthase. Under these conditions, OCR is markedly reduced; the oligomycin-insensitive residual OCR represents leak respiration, whereas the difference between basal and leak OCR provides an indirect estimate of ATP-linked respiration.

The application of a protonophore such as FCCP, which dissipates the protonmotive force and removes its regulatory control over electron transfer, enables the measurement of an OCR typically higher than the basal level. This uncoupled OCR corresponds to the maximal respiratory capacity attainable by the mitochondria, while the difference between uncoupled and

basal OCR is interpreted as the reserve respiratory capacity available under conditions of elevated energetic demand.[27]

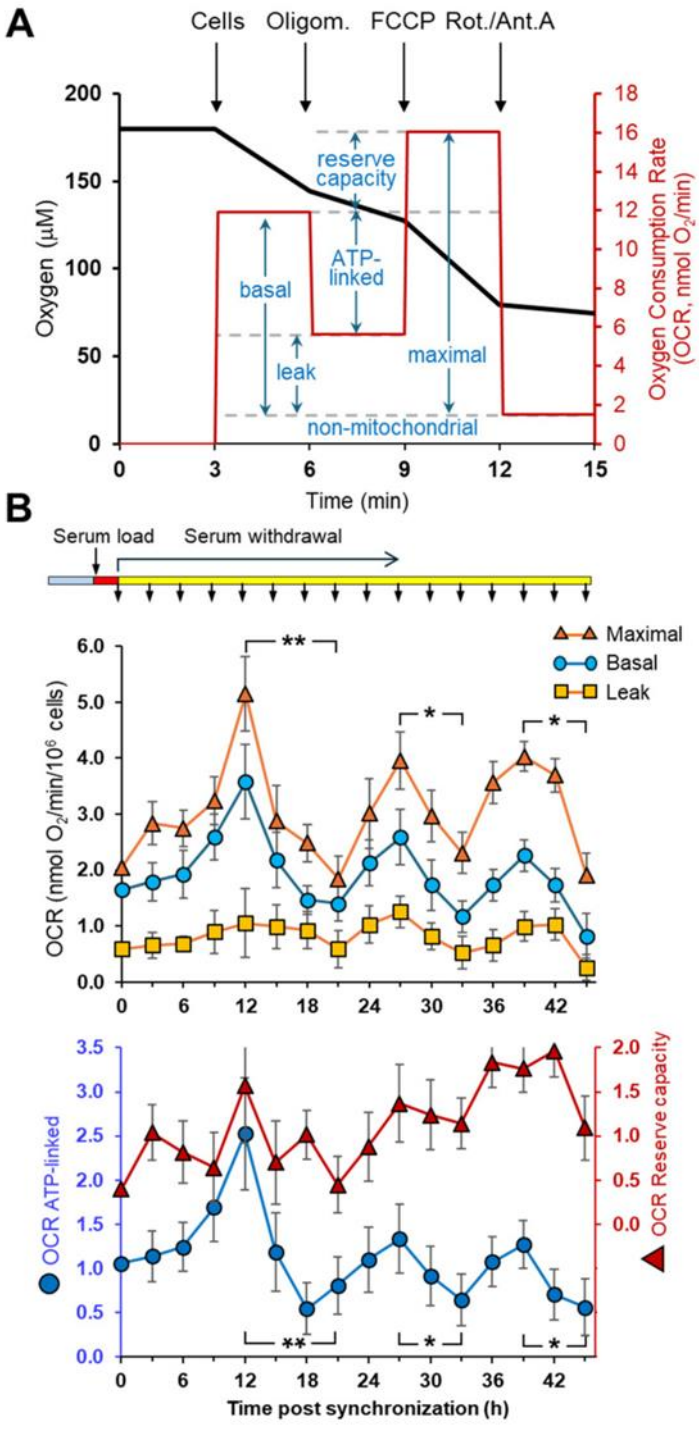

Figure 12: Analysis of mitochondrial respiratory activities in synchronized intact HepG2 cells. (A) Representative oximetric assay using the "mito stress" protocol. Black trace refers to the changes in oxygen content; red trace refers to the rates of oxygen consumption. The upper plot shows the basal, maximal and leak oxygen rates (OCRs) of the cells collected at

the indicated points post-synchronization. The lower plot shows the ATP-linked OCR and the respiratory reserve capacity estimated from the upper panel.[27]

Figure 12A illustrates the sequential "mito stress test,"[28] a protocol designed to extract all previously described respiration-linked parameters. This assay can be performed using classical Clark-type electrodes or more recently developed electrodes containing oxygen-sensitive fluorescent probes [38]. Figure 12A shows the addition of complex I and III inhibitors, rotenone and antimycin A, respectively, which allows the assessment of non-mitochondrial respiration. Subtracting this non-mitochondrial oxygen consumption rate (OCR) from earlier measurements provides the true activity of the mitochondrial respiratory chain.

Figure 12B shows the results of applying the "mito stress test" to the hepatocellular carcinoma cell line HepG2 following in vitro synchronization of the circadian clock. Synchronization was achieved via a serum-shock procedure, in which cells were exposed to 50% serum for 2 hours. Serum removal subsequently synchronized the expression of core clock genes in most cells. At regular intervals post-synchronization (every three hours up to 45 hours), cells were collected and analyzed in suspension using electrode-based oxymetry according to the "mito stress test" protocol.

The upper panel displays raw OCR values corrected for rotenone/antimycin A-insensitive respiration. Basal OCR exhibited spontaneous oscillatory activity, with three peaks within the observation window. Similar oscillatory patterns were observed for OCR leak (in the presence of oligomycin) and maximal OCR (in the presence of FCCP), although their amplitudes were, as expected, lower and higher, respectively. The lower panel shows ATP-linked OCR and spare respiratory capacity calculated from these raw data. ATP-linked OCR maintained an oscillatory pattern like basal OCR, although peak amplitude gradually declined at later timepoints, likely due to progressive loss of synchronization. In contrast, spare respiratory capacity remained largely unchanged over the experimental window.

Substituting the respiratory substrate (glucose with galactose) or using alternative synchronization protocols, such as a brief dexamethasone pulse

followed by washout, similarly elicited rhythmic variations in mitochondrial respiration.[18,27]

4.2 Rhythmic mitochondrial respiration depends on Bmal1 expression

The oscillatory profile in non-synchronized HepG2 cells is markedly dampened, and moreover, BMAL1 silencing inhibits the robustness of oscillatory respiration in synchronized cells, thereby linking mitochondrial respiration to the circadian rhythm of BMAL1.[13]

These results were fully confirmed by following in real-time (i.e., every 15 min) the cellular respiratory activity directly in the microplate, utilizing a recently established new solid-phase optical-sensor detection system (i.e., Resipher) (Figure 13A).

Eighty percent silencing of the Bmal1 expression attained by the siRNA-based approach resulted in a substantial depression/deregulation of the rhythmic activity of mitochondrial respiration, resulting in a reduction in the oscillatory amplitude and elongation of the oscillatory profile.

Mitochondrial respiration and glycolysis were evaluated using Seahorse technology in primary human dermal fibroblasts (NHDF) synchronized by both serum shock and and forskolin treatment (an additional established synchronization protocol)[29]. Both metabolic fluxes displayed a comparable, in-phase oscillatory profile. Accordingly, the resulting "bioenergetic" plot, which correlates basal OCR with basal glycolysis at each time point, revealed a characteristic oscillatory pattern alternating between an energetic and a quiescent state (Figure 13B).[27]

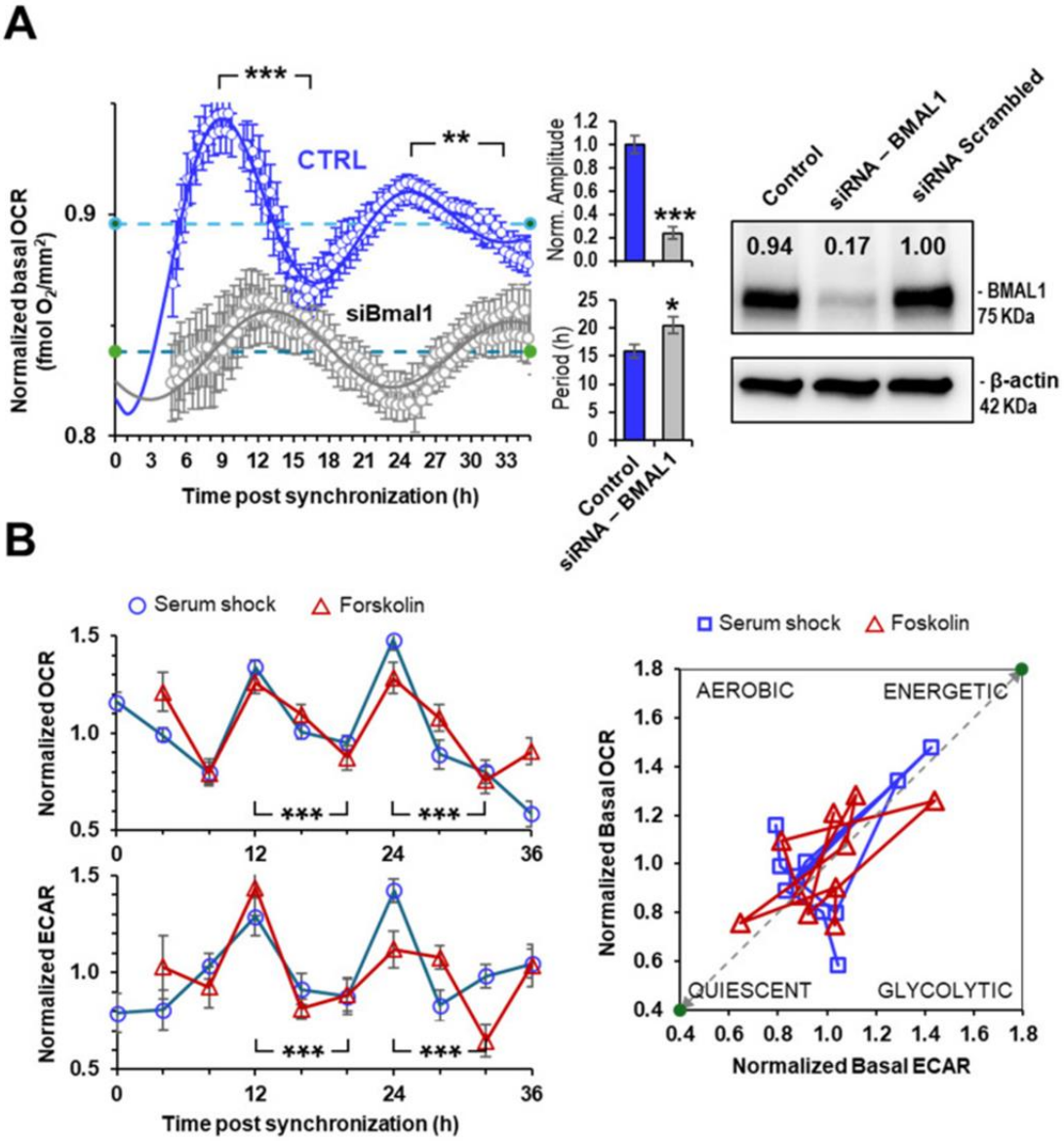

Figure 13: **Measurement of respiratory activities of synchronized cells by Resipher technology and Seahorse technology.** (A) Representative real-time monitoring of the basal OCR on adherent HepG2 cells following serum-shock synchronization by Resipher technology. The blue points (averages of six technical replicates ± SEM) refer to control cells, and the grey points to Bmal1-silenced cells, shown in the western blot on the right side. The bar graphs show the normalized amplitude and the period of the oscillatory OCR profiles in control and siRNA-BMAL1 cells as computed by the Cosinor best-fitting procedure (see text) and refer to three biological replicates: *, $p < 0.05$; **, $p < 0.01$; ***, $p < 0.001$. (B) Representative OCR (upper panel) and ECAR (lower panel) time-resolved profiles in synchronized NHDF assayed by Seahorse technology.[30] Synchronization was performed by either serum shock (blue profiles) or forskolin treatment (red profiles). The points are averages (±SEM) of two biological replicates (four technical replicates/biological replicates) under each condition and were normalized to the mean value of all the time points recorded during the experiment; the statistical significance between the zenith and nadir of two consecutive cycles is shown: ***, $p < 0.001$. The panel on the right shows the bioenergetic plot correlating the normalized OCRs and ECARs from the data indicated in the left panels.[27]

4.3 The autonomous oscillatory profile of mitochondrial respiration differs among different cell types

The observations obtained support the hypothesis that the oscillatory behavior of cellular respiration represents a fundamental mechanism inherent to all cell types. To further characterize this process, several cell samples were analyzed, including primary cells (NHDF), primary immortalized cells (HAEC), tumor cells (HepG2, HeLa, U2OS, Cal27, SCC9), and tumor and metastatic cells originating from the same tissue (SW480 and SW620). For HeLa, U2OS, HepG2, and NHDF, the time-resolved respirometric analysis was performed using the mito stress test, whereas for the remaining cell types only basal OCR values corrected for rotenone-insensitive activity were available, as these samples required a rapid screening focused exclusively on basal OCR.

As shown in Figure 14, respiratory activity was recorded over a 24-hour period at 3-hour intervals following serum-shock synchronization. All cell types exhibited a clear oscillatory pattern of OCR. Notably, when comparing normalized basal OCR and ATP-linked OCR within each cell type, no significant differences were observed in either the overall oscillatory profile or the Cosinor-derived parameters. From a bioenergetic standpoint, this finding indicates that basal OCR can be reliably used as a quantitative descriptor of the oscillatory component of respiration associated with ATP synthesis.

Data were analyzed by nonlinear regression using the Cosinor equation, which provides quantitative estimates of the parameters defining a regular oscillatory profile. These parameters include: the mesor, representing the mean value around which the rhythm oscillates; the amplitude, corresponding to half the peak-to-trough variation; the period, defined as the duration of one full cycle; and the acrophase, indicating the timing of the peak value within the cycle. In our analysis, the amplitude/mesor ratio was used as a normalized parameter, independent of the respiratory phenotype of the different cell samples (Figure 14A).

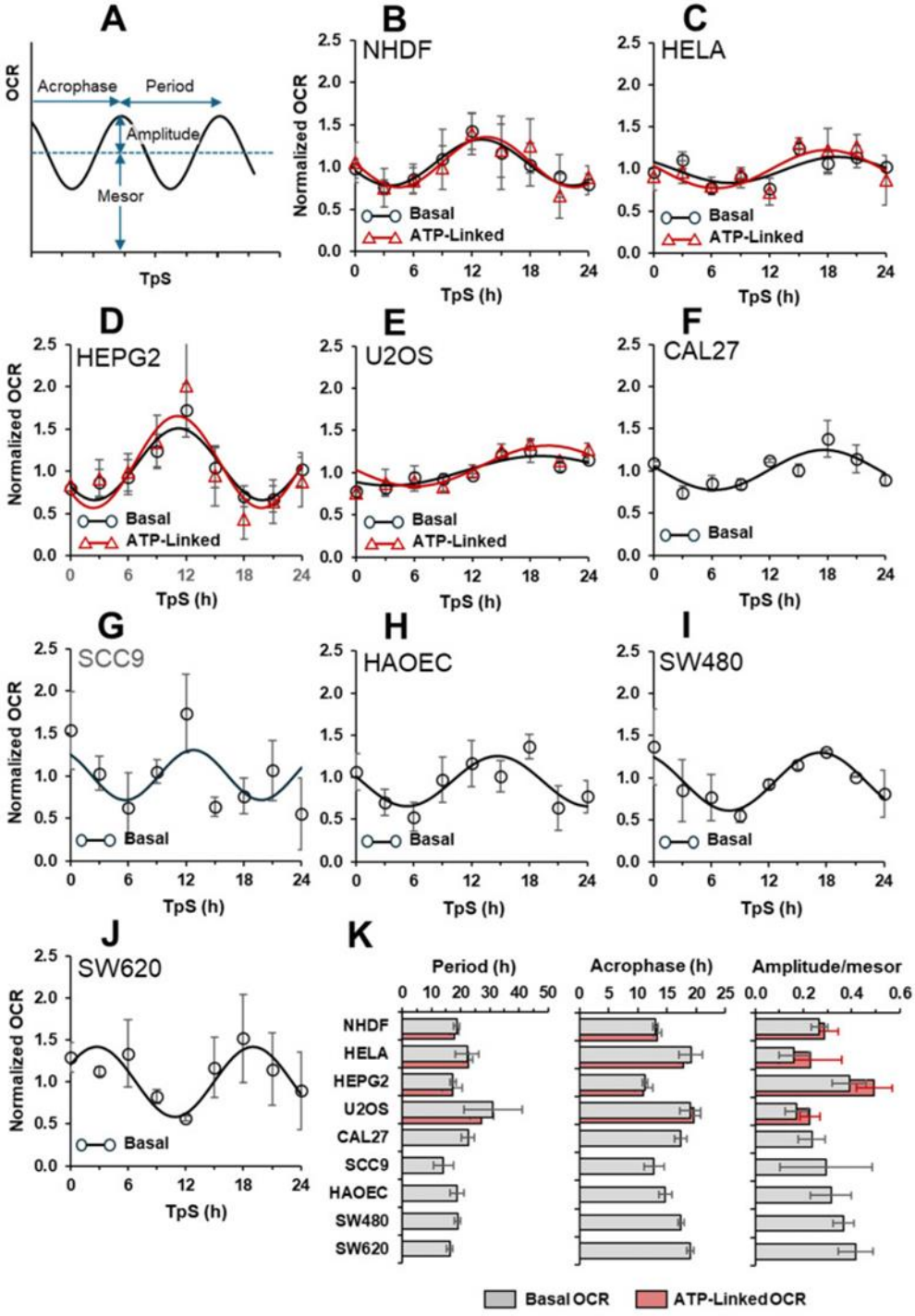

Figure 14: **Cosinor-mediated best-fitting of the OCR profiles in a variety of clock genes synchronized primary cells and cancer-derived cell lines**. (**A**) Scheme showing the parameters of the Cosinor equation in the context of a generic oscillatory rhythm. (**B**–**J**) Best fit of the experimental basal OCRs, measured polarographically in the indicated serum-shock synchronized cells. (**B**–**E**) The ATP-linked OCRs. The points are normalized to the mean value of all the time points recorded during the time course and are the average (±SEM) of at least three independent biological replicates. The continuous lines are the best fit of the experimental points using the Cosinor model with an $\chi^2 < 0.05$. (**K**) Bar graphs showing the triads of Cosinor parameters (i.e., period, acrophase and amplitude/mesor) of the best-fitting curves are shown in panels (**B**–**J**). (The order in which

the cells are shown reflects a progressively decreased value of mitochondrial resting respiration as reported in the next figure).[27]

All analyzed cell types exhibited an autonomous rhythmic pattern of normalized mitochondrial OCR; however, they displayed substantial differences in basal OCR. For this reason, respiratory parameters were correlated with the various Cosinor parameters.

As shown in Figure 15B, no correlation was detected between the duration of the period (ranging from 14 to 31 hours) and basal OCR. Nevertheless, it is worth noting that, with the exception of HeLa and CAL27 cells—whose periods approached the circadian range—all other cell types, regardless of whether they were primary or tumor-derived, exhibited significantly shorter periods, consistent with an ultradian rhythm. An exception was represented by U2OS cells, which displayed a period longer than 24 hours. No correlation was found between the acrophase and basal respiration (Figure 15C). Here as well, the timing of the positive peak was distributed across the different cell samples, occurring between 10- and 20-hours post-synchronization.

Normalized amplitudes were also plotted as a function of basal respiration and, except for the HepG2 cell line, an apparent inverse correlation with an exponential-like trend was observed (Figure 15D). At lower OCR values, the relative oscillation amplitude increased from approximately 15% to 43% relative to the mesor of the respective cell type. Independently of the basal respiratory phenotype, a clearer inverse correlation was detected when relative amplitudes were plotted as a function of the period for each cell type analyzed (Figure 15E).

Comparison of the Cosinor-derived curves fitting the respiratory profiles of the two primary cell types (NHDF and HAEC) with those of the cancer cell lines revealed a marked distinction. Whereas the primary cells displayed nearly superimposable patterns, the tumor-derived lines exhibited a heterogeneous configuration characterized by phase and period misalignment as well as changes in relative amplitude (Figure 16A).[27]

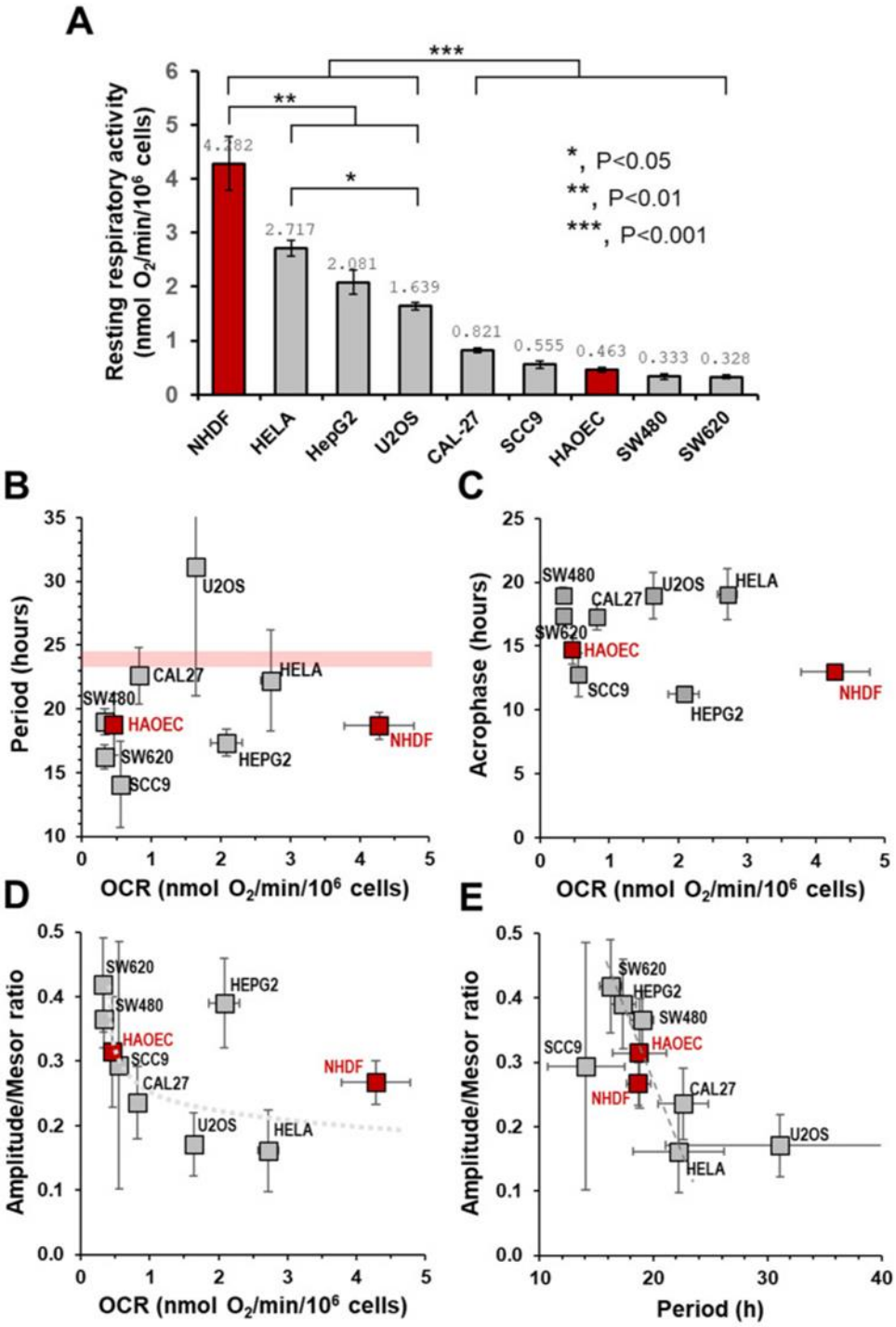

Figure 15: **Correlations between cellular mitochondrial respiratory proficiency and Cosinor-related parameters**. (**A**) The resting/basal OCR is shown for all the indicated cell types used in this study. The values shown refer to the respiratory activity under non-synchronized conditions (not statistically different from the averaged values of the basal OCRs measured during a time course experiment post-synchronization) and are the average (±SEM) of at least five independent biological replicates for each cell type. The statistical analysis of the differences is also shown; for clarity, the statistically significant differences are also indicated between groups of cells. (**B**–**D**) Plots correlating to the respiratory activities of the cell types are shown in panel (**A**), with the Cosinor parameters (i.e., period, acrophase and amplitude/mesor) best fitting the temporal profiles post-

synchronization of the same cell types shown in Figure 14K. The light red line in (**B**) indicates the position in the plot of a canonical circadian oscillation. (**E**) Correlation plot between the Cosinor parameters period and amplitude/mesor best fitting the temporal profiles of the normalized OCRs in the indicated synchronized cells. The red bars in (**A**) and red squares in (**B**–**E**) indicate non-tumor-derived primary cells; the grey bars and squares indicate tumor-derived cell lines.[27]

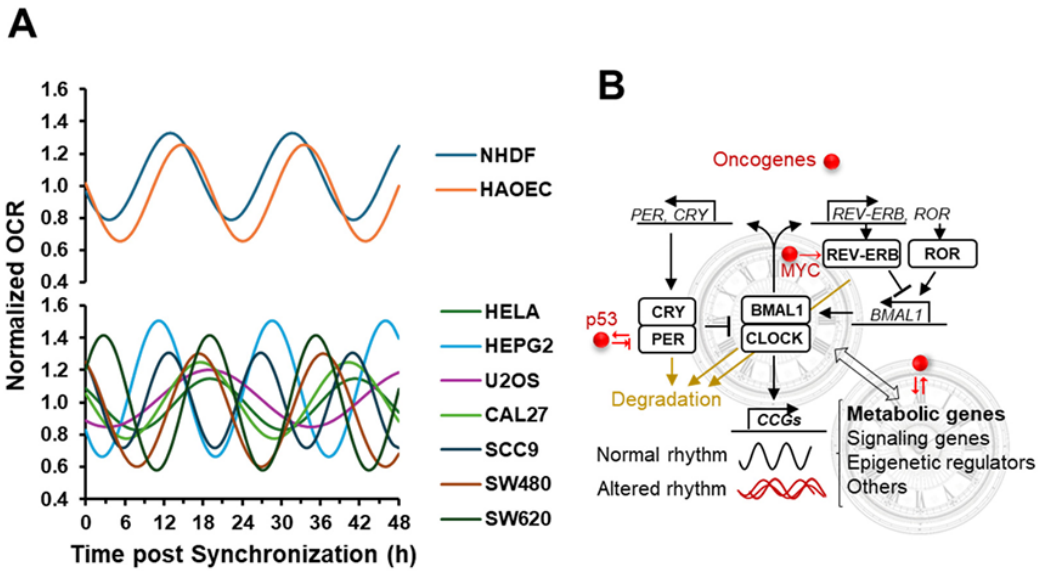

Figure 16: **Comparative analysis of the temporal profiles of mitochondrial respiration in different synchronized cell types.** (**A**) The synchronization-mediated oscillatory OCR profiles of primary cells (upper plot) were compared with those of cancer-derived cell lines. For simplicity, only the Cosinor curves best fitting the experimental data points for the different cell types, shown in Figure 14 B–J, are displayed, and extended to 48 h. (**B**) Schematic drawing of the circadian core clock transcriptional and translational feedback loop and its intertwining with metabolism as well as oncogenes. The red dot indicates oncogenes, with specific mention of those documented to interact with components of the circadian clockwork (i.e., MYC, p53). Oncogenes that regulate various cellular processes, including the expression of genes encoding metabolism-related proteins, are not explicitly marked. The double-headed arrow illustrates a reciprocal interplay between the circadian clockwork and cellular metabolism.[27]

4.4 The transcription of mtDNA genes undergoes spontaneous Bmal1-linked oscillations

Given the link between mitochondrial respiration and Bmal1 expression, the levels of mtDNA-encoded genes were evaluated in serum-shocked synchronized HepG2 cells. The selected genes encode subunits of respiratory Complexes I (ND1), III (CYTB), IV (COXI), and the FoF1 ATP synthase (ATP6). As shown, the transcript levels increased, likely reflecting cell growth, but also displayed an ultradian rhythm with a period of approximately 12 hours. Under these conditions, silencing Bmal1 resulted in a disruption of the rhythmic expression of all mtDNA-encoded genes (Fig. 17B). The efficacy of the BMAL1 siRNA treatment with the BMAL1 expression never >30 % as compared with control (Ctrl) scrambled siRNA. Using the Cosinor equation, the rhythmic parameters were quantified and compared between control and Bmal1-silenced cells. In the silenced samples, the mesors and amplitudes of the cycles were significantly reduced compared to controls. An increase in the periods was also observed (statistically significant for COXI and CYTB), along with a phase delay (acrophase) for all analyzed genes.

It should be noted that the expression of the selected genes occurs via a polycistronic transcript from the heavy strand of mitochondrial DNA, which is subsequently processed into individual mRNAs. The expression of the four genes was averaged and corrected for the upward drift, resulting in a temporally resolved profile with robust oscillatory activity in control cells, which was markedly attenuated in the Bmal1-silenced condition (Fig. 17D).[31]

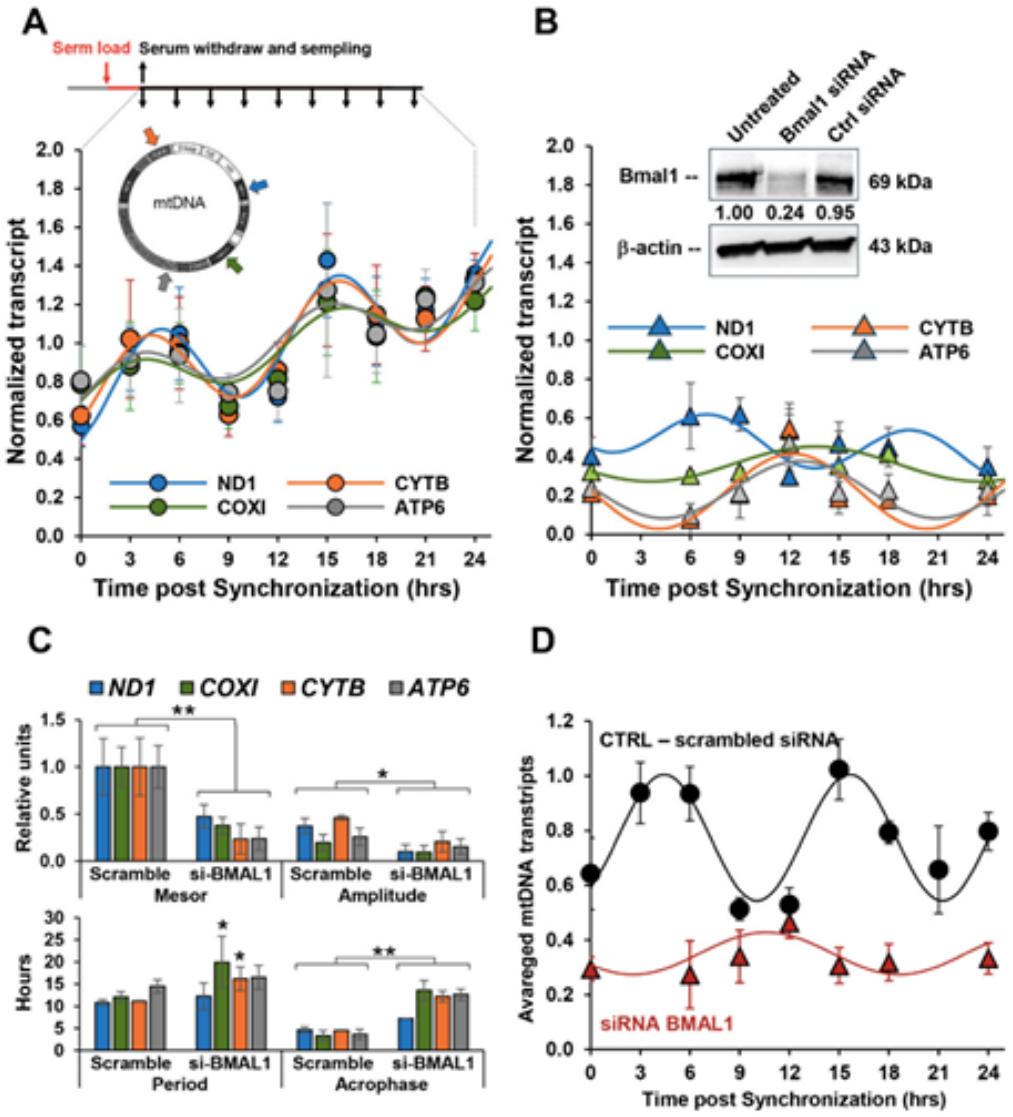

Figure 17: **Expression of mtDNA genes encoding subunits of the respiratory complexes in synchronized HepG2 cells.** (A) Transcript level of genes coding for ND1 (complex I), COX I (complex IV), CYTB (complex III), ATP 6 (complex V/ATP synthase) are shown at the indicated timepoints post-synchronization. The values shown were normalized to the average of all the data-points in a time series and are means ± SEM of 4 different independent experiments. The mitochondrial DNA shown in the insert indicates the position of the genes assessed. (B) Experimental conditions as in (A) but with HepG2 cells silenced for the expression of the clock gene BMAL1. (C) Statistical analysis of the parameters shaping the oscillatory profiles, shown in (A) and (B) as inferred from the Cosinor analysis. The Mesor and Amplitude in silenced BMAL1 (siBMAL1) were normalized to the Mesor values attained with scrambled siRNA. *, $P < 0.05$; **, $P < 0.01$. (D) Averaged transcript level of the four selected genes, according to the polycistronic modality of the mtDNA expression, in control and siRNA BMAL1 cells. The timepoints series were corrected for the slopes highlighting the rhythmic profiles of the transcripts in control cells.[31]

4.5 The expression of factors controlling mitochondrial biogenesis undergoes spontaneous Bmal1-linked oscillations though the content of the mitochondrial respiratory complexes does not change

Since mitochondrial DNA (mtDNA) expression is known to be regulated by nuclear transcription factors, we primarily examined the expression of the PPARGC1A gene, which encodes the transcriptional coactivator PGC1α, and consequently the expression of the transcription factors NRF1 and TFAM. These genes were analyzed in synchronized HepG2 cells and in HepG2 cells treated with Bmal1 siRNA.

Consistent with the other results, the expression of these three genes—which together constitute the core regulatory module of mitochondrial biogenesis—displayed rhythmic oscillations that were attenuated upon BMAL1 silencing (Figure 18A, B, C). Cosinor analysis enabled the detection of statistical differences in rhythmic parameters between control and Bmal1-silenced cells (Figure 18D).

Given these observations, one would expect the respiratory complexes to also exhibit oscillatory protein expression following synchronization. However, blue native electrophoretic analysis of mitochondria isolated from HepG2 cells at three post-synchronization time points did not reveal any differences in the abundance of the OXPHOS complexes (data not shown, as these were generated prior to the present project).

This finding was confirmed by a systematic Western blot analysis assessing the protein levels of nuclear-encoded and mtDNA-encoded subunits of Complex I (ND1 and NDUFB8) and Complex IV (COXII and COXIV). Figures 19A and 19B show that there were no significant changes in the abundance of Complex I and Complex IV subunits, nor any oscillatory profiles after synchronization, regardless of their genomic origin.[31]

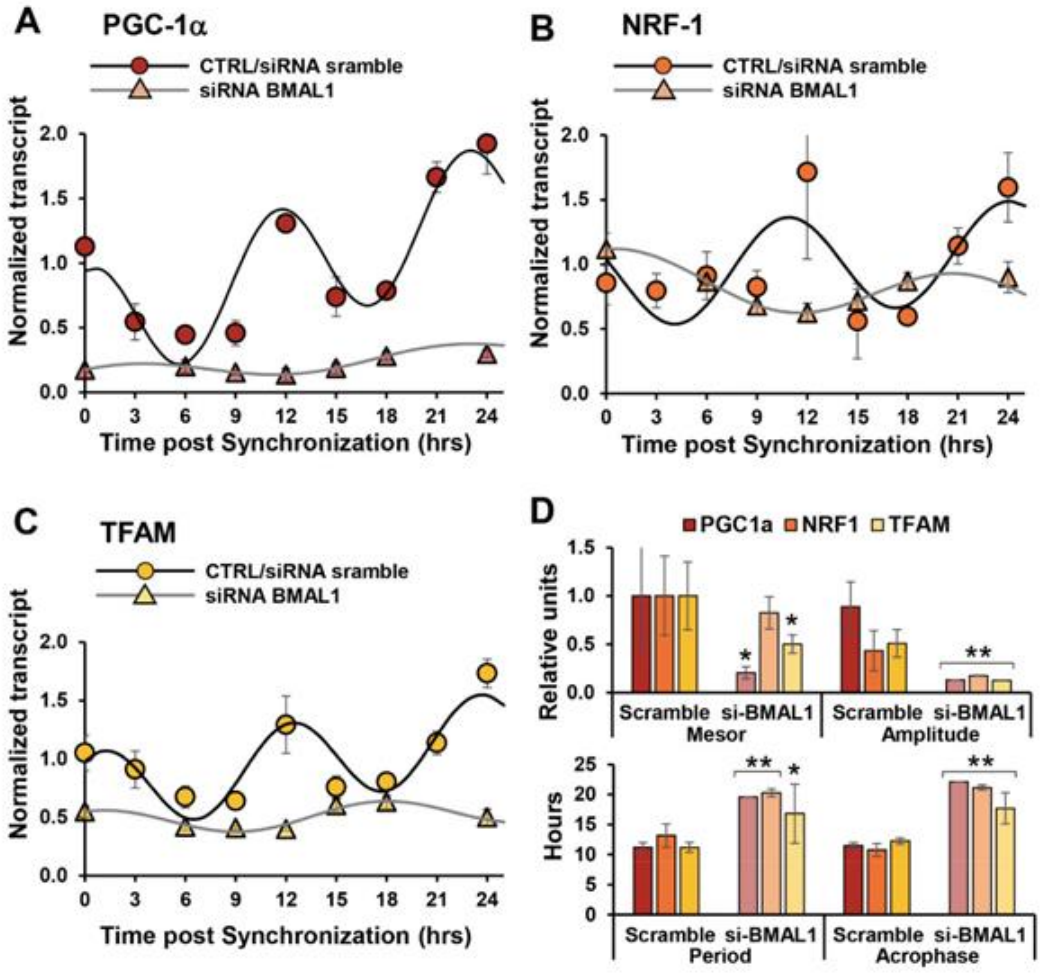

Figure 18: Time-resolved expression of nuclear genes encoding factors involved in the biogenesis of mitochondria in synchronized HepG2 cells. The graphs in (A), (B) and (C) show the transcript levels of genes coding for PGC-1a, NRF1 and TFAM, respectively. The values are means ± SEM of 4 different independent experiments and the lines are the non-linear Cosinor best fits (as in Fig. 1). (D) Statistical analysis of the parameters shaping the oscillatory profiles, shown in (A), (B) and (C) as inferred from the Cosinor analysis. The Mesor and Amplitude in silenced BMAL1 (siBMAL1) were normalized to the Mesor values attained with scrambled siRNA. *, $P < 0.05$ and **, $P < 0.01$ vs respective mock.[31]

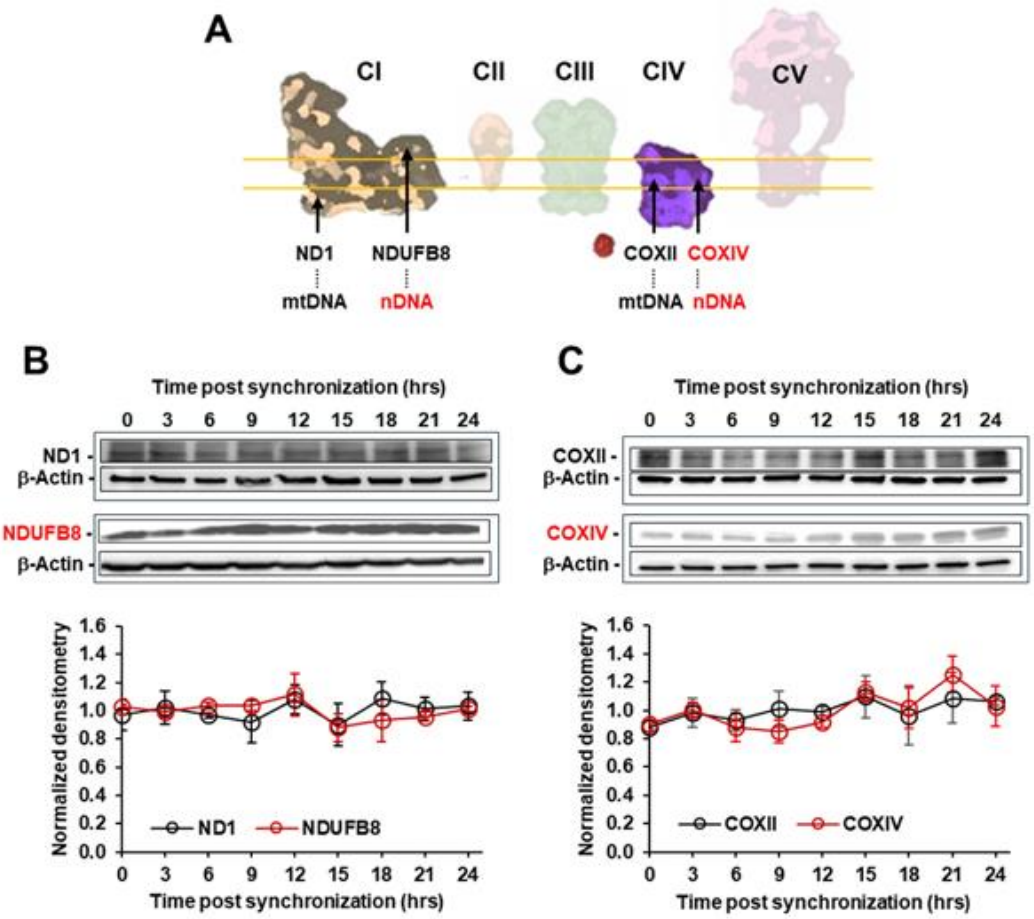

Figure 19: Time-resolved expression of selected protein subunits of the respiratory Complexes I and IV in synchronized HepG2 cells. The upper drawing (A) shows schematically the respiratory Complexes and the approximate location of the nuclear and mitochondrial DNA coded subunits the object of the analysis. Western blotting is representative for the immune detection of the mtDNA- and nuclear-DNA encoded subunits ND1 and NDUFB8, respectively, of complex I (B) and for the mtDNA- and nuclear-DNA encoded subunits COXII and COXIV, respectively, of complex IV (C). The graphs below the Western blottings show the densitometric analysis of three independent assays for each subunit with values normalized to the averaged data-point series and reported as means ± SEM at each time point.[31]

4.6 The expression of factor controlling mitochondrial quality control and mitochondrial biogenesis undergoes spontaneous oscillations

Mitochondria undergo a mitophagic quality control process that leads to their selective degradation. Considering the evidence of circadian rhythmic mitophagic activity, we investigated this process in our cellular model. Protein levels of LC3-I and LC3-II were assessed in synchronized HepG2 cells over time by Western blotting. Densitometric analysis showed that the LC3-II isoform displays an oscillatory profile. The same samples were analyzed for PGC-1α protein content, which also exhibited a rhythmic pattern, consistent with the mRNA expression analysis shown in Figure 18A. Notably, the analysis of the rhythmic parameters of the oscillatory patterns of PGC-1α and LC3 revealed no statistically significant differences in either the oscillation period or acrophase. The rhythmic activities of these two proteins suggest that mitochondrial biogenesis and degradation occur synchronously, that is, in phase, thereby contributing to the maintenance of steady-state mitochondrial protein levels, including those of the OXPHOS machinery.

Mitophagy is closely associated with changes in mitochondrial morphology, mitochondria become more fragmented during this process. Figure 20D shows confocal images of the mitochondrial network in HepG2 cells stained with the mitotropic fluorescent probe TMRE. Three time points after synchronization were selected: the peak of LC3 activation (6 h) and the two flanking nadirs (0 and 12 h). The enlarged images clearly show a change in the morphology of the mitochondrial fluorescence signal, which appears more punctuated at 6 h post-synchronization compared with the more interconnected features observed at 0 and 12 h. Morphometric analysis statistically confirmed these observations (Fig. 20E).[31]

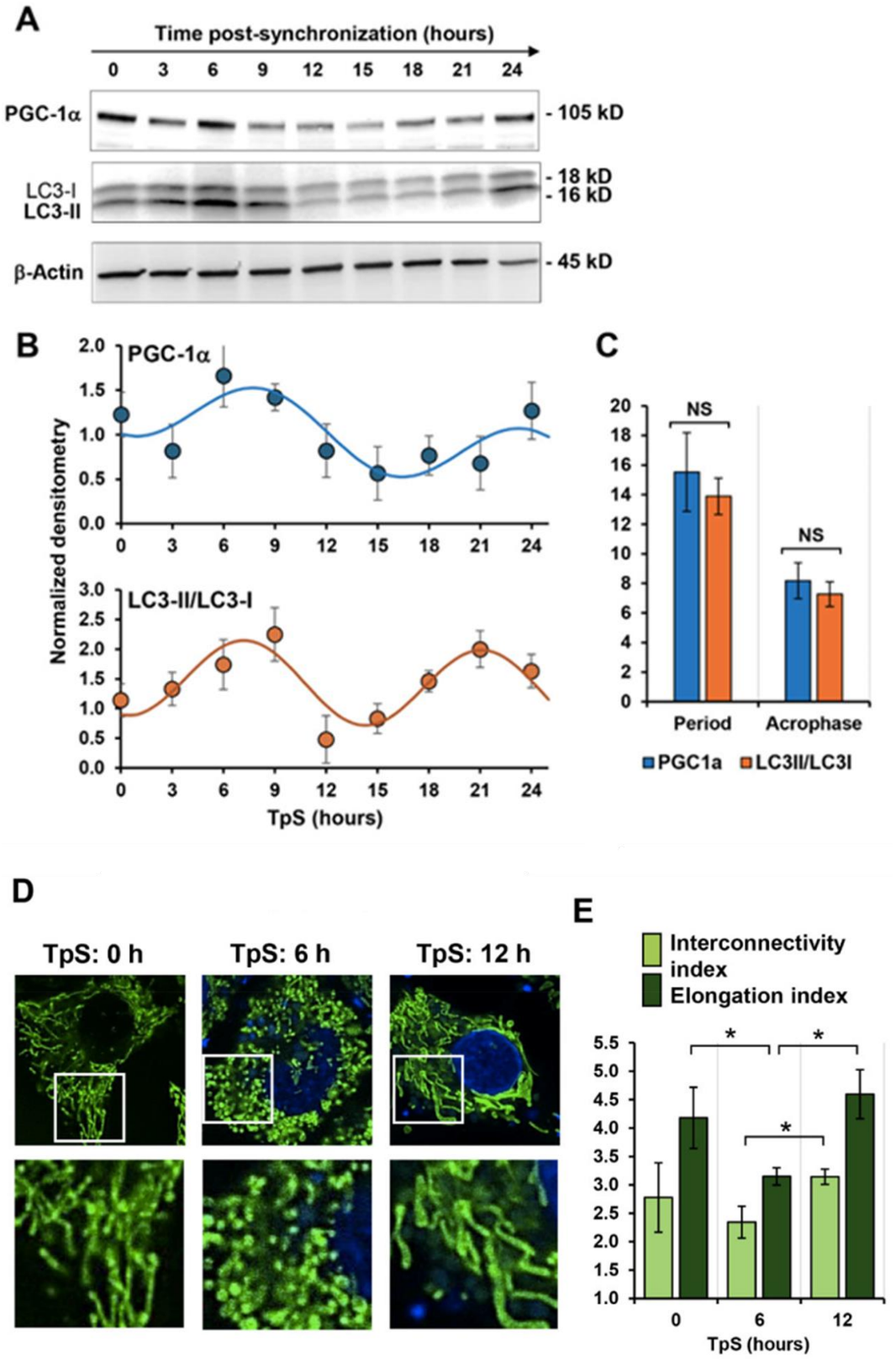

Figure 20: Time-resolved expression of proteins involved in mitochondrial biogenesis and degradation in synchronized HepG2 cells. (A) Representative Western blotting for immune detection of PGC-1a and LC3-I/II. (B) Densitometric analysis of three independent WB assays as in (B) for each subunit with values normalized to the averaged data-point series and reported as means ± SEM at each time point. The curves throughout the data-points

are the non-linear Cosinor best fits with the parameters period and amplitude shown in (C). (D) Representative confocal microscopy of cell stained with Mito Tracker green imaged at the indicated time points post synchronization (TpS). Enlarged details of the cells are also shown. (E) Results of the morphometric analysis of the mitochondrial network showing the interconnectivity and elongation indexes. The bars are the averages ± SEM of at least 30 cell images casually selected from each of three biological replicates. *, P < 0.05.[31]

4.7 The expression of factors controlling mitochondrial dynamics undergoes spontaneous oscillation

Mitochondrial dynamics are regulated by organelle fusion and fission processes, which are also subject to circadian regulation. The study was therefore expanded by assessing the factors involved in mitochondrial fusion (i.e., mitofusins 1 and 2, and OPA1) and fission (DRP1).

Synchronized HepG2 cells exhibited an oscillatory pattern in the protein levels of mitofusin 2 (MFN2) (Fig. 6A). In contrast, the temporal expression of mitofusin 1 (MFN1) remained relatively stable, showing no significant variation.

The expression of OPA1, in both its membrane-inserted and cleaved soluble forms (L-OPA1 and S-OPA1, respectively), also displayed an oscillatory pattern, though with a phase distinct from that of MFN2.

Furthermore, the analysis of DRP1 revealed a rhythmic oscillation that was nearly in anti-phase relative to MFN2. These observations suggest an alternating regulation of mitochondrial fusion and fission in HepG2 cells.

A similar analysis performed in another cell line, U2OS, revealed comparable oscillatory patterns in mitochondrial fusion, fission, and mitophagy factors, although some phase differences were observed.[31]

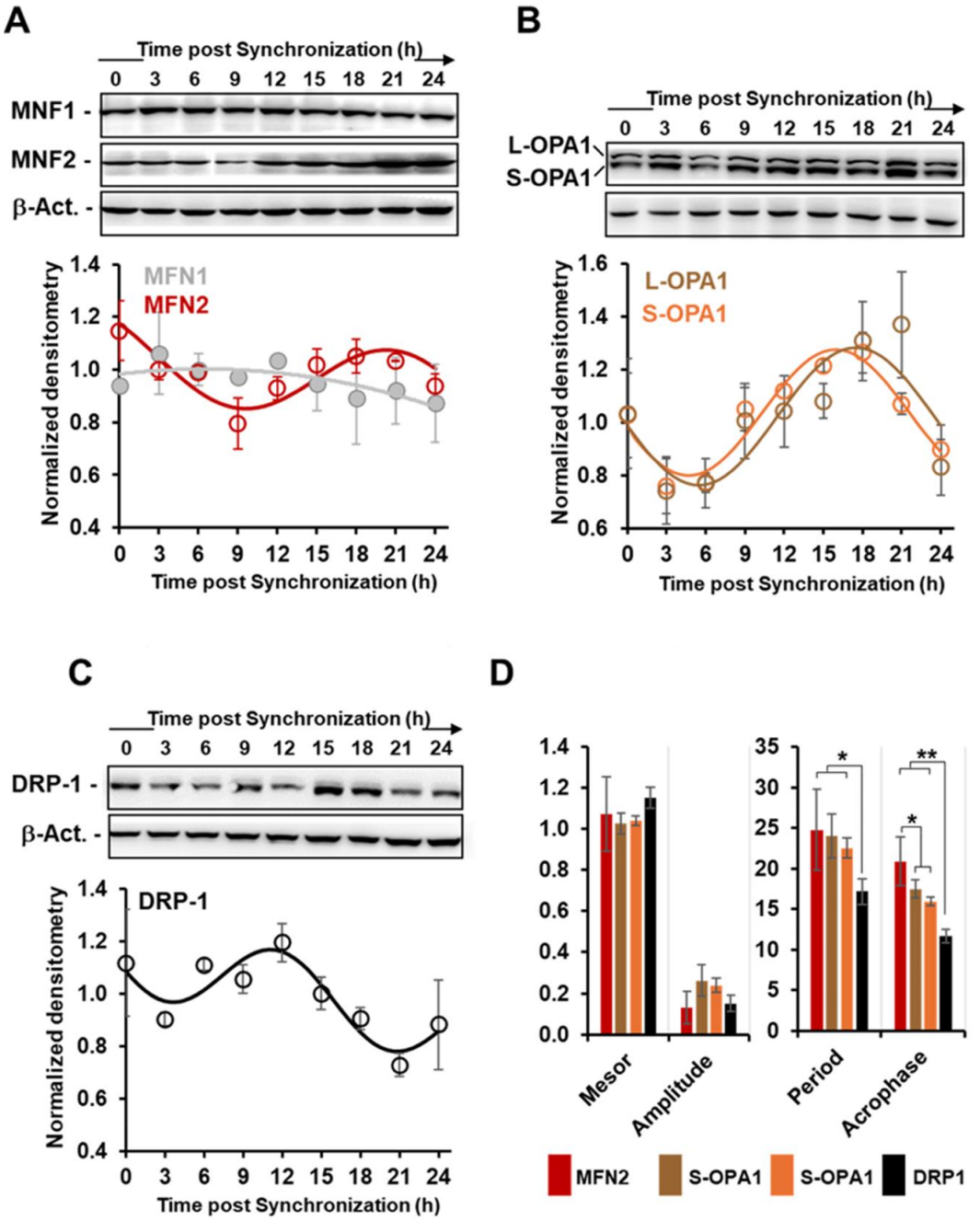

Figure 21: Time resolved expression of proteins involved in fusion/fission of the mitochondrial network in synchronized HepG2 cells. Representative Western blottings for immune detection of MFN1 and MFN2 (A), long L-OPA1 and short S-OPA1 (B) and DRP1 (C) are shown. The graphs below each blot show the densitometric analysis of three independent WB assays for each protein with values normalized to the averaged data-point series and reported as means ± SEM at each time point. The curves throughout the data-points are the non-linear Cosinor best fits. (D) Statistical analysis of the parameters shaping the oscillatory profiles, shown in (A)-(C) as inferred from the Cosinor analysis. The Amplitudes were normalized to the Mesor values of each protein. *, $P < 0.05$; **, $P < 0.01$.[31]

5. DISCUSSION AND CONCLUSION

The efficiency of electron transfer in the mitochondrial respiratory chain, essential for ATP synthesis, can be assessed by measuring oxygen consumption both in isolated mitochondria and in intact cultured cells. In previous studies, using polarographic methods, it was demonstrated that cellular respiration attributable to the mitochondrial electron transport chain exhibits an autonomous and robust oscillatory activity after in-vitro synchronization. As shown in Figure 12A and B, the oligomycin-sensitive OCR (ATP-linked oxygen consumption) also retains an oscillatory pattern. In contrast, the spare respiratory capacity does not display an oscillatory profile, since maximal respiration varied in parallel with basal respiration, maintaining an almost constant difference between the two. This phenomenon is independent of the respiratory carbon source, synchronization protocol, analytical method used, and cellular model examined (including both primary cells such as NHDF and cancer cells such as HepG2). Furthermore, oscillatory respiratory activity was found to be associated with the expression of BMAL1, a master circadian clock gene.[18] To validate the data previously obtained by polarography, additional methods for measuring OCR were employed. In Figure 13A, a recently developed technique was used that relies on an O_2-sensitive fluorescent probe to monitor OCR in real time directly in microplates following in-vitro synchronization, without the need to detach or resuspend the cells. The resulting profile fully confirmed the findings obtained with the traditional oxygraphic method on suspended cells and revealed an attenuated oscillatory pattern in BMAL1-silenced cells, further supporting the link between circadian clock gene expression and mitochondrial respiratory activity. Using Seahorse technology, both respiratory and glycolytic fluxes exhibited in-phase oscillatory activity, with no compensatory upregulation of one pathway in response to downregulation of the other (Figure 13B). Among the different cell types analyzed (Figure 14), basal respiration showed considerable variability across samples in both primary and tumor-

derived cells. Data analyzed using the Cosinor equation (a function relating the main parameters underlying oscillatory profiles) revealed significant differences in period, acrophase, and amplitude/mesor ratio between basal OCR and ATP-linked OCR within the same cell type, supporting the use of normalized basal OCR as a reliable indicator of functional respiratory oscillation.

A key result emerging from comparative analysis is the variability of the oscillatory period of mitochondrial respiration, ranging from 24 hours to shorter periods (Figure 15B). These results suggest differential regulations of rhythmic mitochondrial respiration depending on cellular phenotype or genotype.

Comparison of Cosinor parameters revealed a highly heterogeneous scenario and attempts to correlate these parameters with different respiratory phenotypes did not yield significant relationships. The only relevant association was an inverse correlation between relative oscillation amplitude and period within each cell type, independent of absolute respiratory rate (Figure 14).

A noteworthy comparison concerns Cosinor-derived curves obtained for the two primary cell types (NHDF and HAEC) versus those of tumor cell lines: while primary cells displayed nearly superimposable patterns, tumor cells exhibited a heterogeneous configuration characterized by phase and period misalignment and variations in relative amplitude (Figure 16A). The heterogeneity of circadian rhythms in tumor cells represents a biologically and clinically relevant aspect of tumor biology. As illustrated in Figure 16B, several proto-oncogenes are under circadian control. Although the circadian clock regulates essential physiological processes in healthy cells, including metabolism, proliferation, and DNA repair, tumor cells often display altered or disrupted circadian rhythms. Such heterogeneity may significantly affect tumor growth, treatment response, and clinical outcomes.

To further investigate cellular respiration, the expression of four mtDNA-encoded genes, corresponding to the catalytic subunits of complexes I, III, and IV and to a subunit of complex V (FoF1-ATP synthase), was examined. After in-vitro synchronization, all four selected transcripts exhibited a

similar oscillatory profile, reflecting the polycistronic mode of mtDNA expression. The average content of these transcripts at different time points post-synchronization revealed a robust rhythmic profile. Cosinor analysis quantified an ultradian period (~12 h) with a relative amplitude of 0.25 (normalized to the mesor), corresponding to an approximate doubling of transcript levels between nadir and subsequent zenith. Rhythmic mtDNA transcription was markedly attenuated and dysregulated when BMAL1 expression was silenced by ~75%, indicating a link with the circadian system. Notably, the loss of rhythmicity in mitochondrial transcripts in BMAL1-silenced cells was accompanied by an overall reduction in the transcriptional activity of the mitochondrial genes analyzed (Figure 17).

Paradoxically, the protein content of the respiratory complexes did not show significant variation at different times post-synchronization. Moreover, except for complex I, no other respiratory chain complex displayed a rhythmic profile.[13] This suggests that the rhythmic activity of complex I may depend on a reversible post-translational modification (acetylation/deacetylation) affecting complex I and thereby influencing the rhythmicity of cellular respiratory activity.[13] The deacetylation/activation phase of complex I appears largely responsible for the increased respiratory activity at oscillatory peaks. This process was mediated by the rhythmic and coordinated expression of the deacetylases SIRT1 and SIRT3 and by the levels of oxidized NAD^+, which in turn depend on the rhythmic expression of NAMPT, directly regulated by the CLOCK/BMAL1 heterodimer.

Cellular respiration reflects mitochondrial homeostasis and metabolism. In this thesis, mitochondrial dynamics (fusion and fission), biogenesis, and mitophagy were also evaluated in the context of circadian regulation. Transcripts belonging to the PGC-1α → NRF1 → TFAM transcriptional cascade regulating mitochondrial biogenesis were analyzed and all displayed oscillatory profiles that were abolished in BMAL1-siRNA–treated cells (Figure 18).

While PGC-1α regulates biogenesis, LC3 is involved in mitophagy. Protein profiles displayed oscillatory and in-phase behavior. This finding was corroborated by confocal microscopy using a fluorescent probe, which

revealed rhythmic changes in mitochondrial morphology, alternating between more fragmented configurations and more elongated, tubular, interconnected networks. Notably, the fragmented mitochondrial network was approximately in phase with the expression peaks of LC3-II and PGC-1α. This oscillation between biogenesis and mitophagy ensures maintenance of mitochondrial number (Figure 20).

To investigate mitochondrial fission and fusion, protein levels of the main regulators, DRP1, MFN1, MFN2, and OPA1, were analyzed. The data show that their expression follows oscillatory patterns, but with asynchronous phases. It is noteworthy that MFN2 and OPA1 exhibit oscillatory expression profiles with distinct phases, suggesting temporally separate regulation of the two ~24-hour mitochondrial membrane fusion processes (Figure 21).

An important aspect emerging from the analyses is that the expression of core clock genes displays a circadian period (~24 h), whereas the transcription of other clock-controlled genes, such as mtDNA-encoded genes, shows ultradian oscillation (~12 h). This phenomenon may depend on multiple factors: if the expression of a given gene requires the simultaneous presence of two or more factors, the output will depend on the combination of their phases. For instance, if two circadian transcription factors differ by ~12 h in phase, their concentrations will converge every ~12 h, and their target gene will therefore exhibit maximal expression with an ultradian rhythm.

Another possible contributing mechanism involves reversible post-transcriptional or post-translational modifications, or RNA-silencing mechanisms, that shift the phase of proteins with circadian rhythmicity. Further studies will be required to clarify these hypotheses.[27,31]

A final hypothesis is the existence of a distinct rhythmic system regulating ultradian rhythms, operating wholly or partly independently of the canonical circadian system. Further investigations will be needed to validate this possibility. One way to interpret the oscillation of oxygen consumption in the absence of temporal changes in the protein levels of respiratory chain subunits (Figure 19) is to consider that the mitochondrial population itself varies over time. A balanced equilibrium, controlled by the circadian clock,

exists between biogenesis and mitophagy. Mitochondrial morphology also changes over time through fission and fusion processes. Indeed, mitochondrial dynamics oscillate, alternating between a fragmented mitochondrial network and more tubular, interconnected mitochondria. These equilibria, particularly between biogenesis and mitophagy, may explain the stability of respiratory chain subunit protein levels and suggest another form of oscillatory regulation of OXPHOS that may depend on the temporal regulation of post-translational modifications of respiratory chain subunits. These results support the hypothesis that Circadian Clock Machinery controls OxPHOS proteostasis by coordinating mitochondrial biogenesis and mitophagy as well as mitochondrial dynamics.

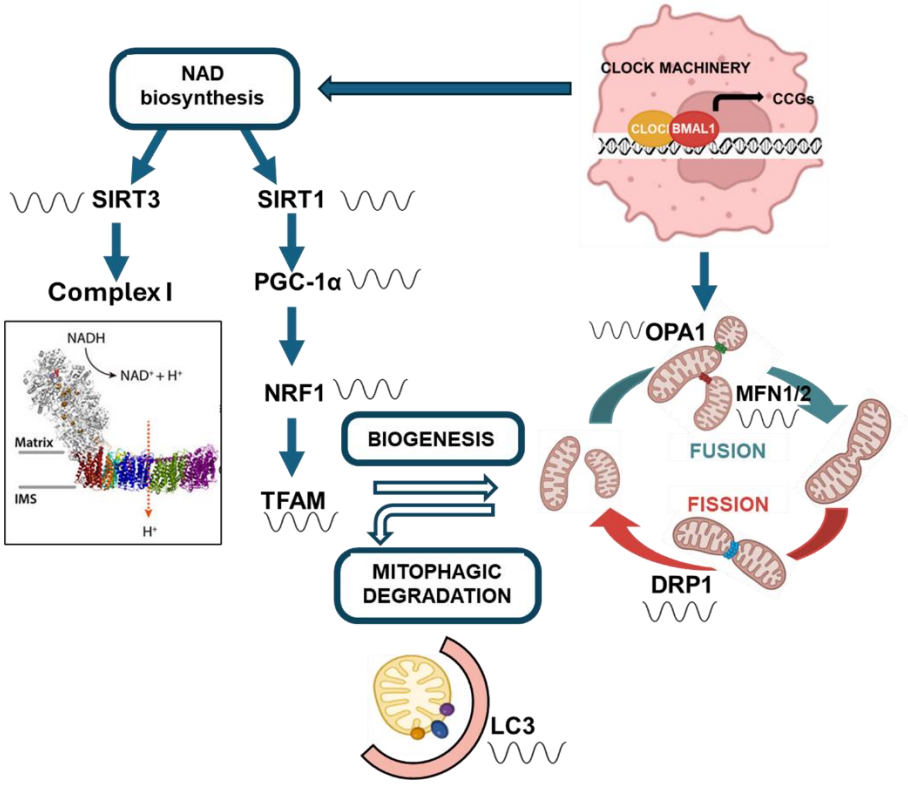

Figure 22: Representation of the suggested circadian control of mitochondrial biogenesis vs mitophagy and fusion vs fission balance.

6. REFERENCES

1. Guan D, Lazar MA. Interconnections between circadian clocks and metabolism. *J Clin Invest*. 2021;131(15):e148278. doi:10.1172/JCI148278
2. Paschos GK, FitzGerald GA. Circadian clocks and Metabolism: implications for microbiome and aging. *Trends Genet TIG*. 2017;33(10):760-769. doi:10.1016/j.tig.2017.07.010
3. Mazzoccoli G, Pazienza V, Vinciguerra M. Clock Genes and Clock-Controlled Genes in the Regulation of Metabolic Rhythms. *Chronobiol Int*. 2012;29(3):227-251. doi:10.3109/07420528.2012.658127
4. Hastings MH, Maywood ES, Brancaccio M. Generation of circadian rhythms in the suprachiasmatic nucleus. *Nat Rev Neurosci*. 2018;19(8):453-469. doi:10.1038/s41583-018-0026-z
5. Koronowski KB, Sassone-Corsi P. Communicating clocks shape circadian homeostasis. *Science*. 2021;371(6530):eabd0951. doi:10.1126/science.abd0951
6. Morin R, Forest G, Imbeault P. Circadian rhythms revealed: unraveling the genetic, physiological, and behavioral tapestry of the human biological clock and rhythms. *Front Sleep*. 2025;4. doi:10.3389/frsle.2025.1544945
7. Transcriptional architecture of the mammalian circadian clock | Nature Reviews Genetics. Accessed April 11, 2022. https://www.nature.com/articles/nrg.2016.150

8. Reinke H, Asher G. Crosstalk between metabolism and circadian clocks. *Nat Rev Mol Cell Biol*. 2019;20(4):227-241. doi:10.1038/s41580-018-0096-9

9. Gopalakrishnan S, Kannan NN. Only time will tell: the interplay between circadian clock and metabolism. *Chronobiol Int*. 2021;38(2):149-167. doi:10.1080/07420528.2020.1842436

10. Manella G, Asher G. The Circadian Nature of Mitochondrial Biology. *Front Endocrinol*. 2016;7. Accessed April 19, 2022. https://www.frontiersin.org/article/10.3389/fendo.2016.00162

11. Yusri K, Jose S, Vermeulen KS, Tan TCM, Sorrentino V. The role of NAD+ metabolism and its modulation of mitochondria in aging and disease. *Npj Metab Health Dis*. 2025;3(1):26. doi:10.1038/s44324-025-00067-0

12. Houtkooper RH, Cantó C, Wanders RJ, Auwerx J. The Secret Life of NAD+: An Old Metabolite Controlling New Metabolic Signaling Pathways. *Endocr Rev*. 2010;31(2):194-223. doi:10.1210/er.2009-0026

13. Cela O, Scrima R, Pazienza V, et al. Clock genes-dependent acetylation of complex I sets rhythmic activity of mitochondrial OxPhos. *Biochim Biophys Acta BBA - Mol Cell Res*. 2016;1863(4):596-606. doi:10.1016/j.bbamcr.2015.12.018

14. Imai S ichiro, Guarente L. NAD+ and Sirtuins in Aging and Disease. *Trends Cell Biol*. 2014;24(8):464-471. doi:10.1016/j.tcb.2014.04.002

15. Menger KE, Rodríguez-Luis A, Chapman J, Nicholls TJ. Controlling the topology of mammalian mitochondrial DNA. *Open Biol*. 2021;11(9):210168. doi:10.1098/rsob.210168

16. Anand S, Balgote PJ, Sivaraman J. Exploring the connection between the Mitochondrial DNA and the Circadian Rhythm: Insights into Mitochondrial Biogenesis and its Dynamics. *Mol Biol Rep*. 2025;52(1):971. doi:10.1007/s11033-025-11010-3

17. de Goede P, Wefers J, Brombacher EC, Schrauwen P, Kalsbeek A. Circadian rhythms in mitochondrial respiration. *J Mol Endocrinol*. 2018;60(3):R115-R130. doi:10.1530/JME-17-0196

18. Scrima R, Cela O, Merla G, et al. Clock-genes and mitochondrial respiratory activity: Evidence of a reciprocal interplay. *Biochim Biophys Acta BBA - Bioenerg*. 2016;1857(8):1344-1351. doi:10.1016/j.bbabio.2016.03.035

19. Rodríguez-Córdoba KM, Soto SA, Garzón JAC, Pustovrh-Ramos MC. Mitochondrial dynamics, biogenesis, mitophagy and oxidative stress in gestational obesity: A review. *Endocr Metab Sci*. 2025;17:100205. doi:10.1016/j.endmts.2024.100205

20. Triolo M, Hood DA. Mitochondrial breakdown in skeletal muscle and the emerging role of the lysosomes. *Arch Biochem Biophys*. 2019;661:66-73. doi:10.1016/j.abb.2018.11.004

21. Jacobi D, Liu S, Burkewitz K, et al. Hepatic Bmal1 regulates rhythmic mitochondrial dynamics and promotes metabolic fitness. *Cell Metab*. 2015;22(4):709-720. doi:10.1016/j.cmet.2015.08.006

22. de Goede P, Wefers J, Brombacher EC, Schrauwen P, Kalsbeek A. Circadian rhythms in mitochondrial respiration. *J Mol Endocrinol*. 2018;60(3):R115-R130. doi:10.1530/JME-17-0196

23. Tilokani L, Nagashima S, Paupe V, Prudent J. Mitochondrial dynamics: overview of molecular mechanisms. *Essays Biochem*. 2018;62(3):341-360. doi:10.1042/EBC20170104

24. Al Ojaimi M, Salah A, El-Hattab AW. Mitochondrial Fission and Fusion: Molecular Mechanisms, Biological Functions, and Related Disorders. *Membranes*. 2022;12(9):893. doi:10.3390/membranes12090893

25. Kim J, Sun W. Circadian coordination: understanding interplay between circadian clock and mitochondria. *Anim Cells Syst*. 28(1):228-236. doi:10.1080/19768354.2024.2347503

26. Balsalobre A, Damiola F, Schibler U. A Serum Shock Induces Circadian Gene Expression in Mammalian Tissue Culture Cells. *Cell*. 1998;93(6):929-937. doi:10.1016/S0092-8674(00)81199-X

27. Cela O, Scrima R, Pacelli C, Rosiello M, Piccoli C, Capitanio N. Autonomous Oscillatory Mitochondrial Respiratory Activity: Results of a Systematic Analysis Show Heterogeneity in Different In Vitro-Synchronized Cancer Cells. *Int J Mol Sci*. 2024;25(14):7797. doi:10.3390/ijms25147797

28. Brand MD, Nicholls DG. Assessing mitochondrial dysfunction in cells. *Biochem J*. 2011;435(Pt 2):297-312. doi:10.1042/BJ20110162

29. Balsalobre A, Marcacci L, Schibler U. Multiple signaling pathways elicit circadian gene expression in cultured Rat-1 fibroblasts. *Curr*

Biol CB. 2000;10(20):1291-1294. doi:10.1016/s0960-9822(00)00758-2

30. Pacelli C, Rotundo G, Lecce L, et al. Parkin Mutation Affects Clock Gene-Dependent Energy Metabolism. *Int J Mol Sci*. 2019;20(11):2772. doi:10.3390/ijms20112772

31. Cela O, Scrima R, Rosiello M, et al. Circadian clockwork controls the balance between mitochondrial turnover and dynamics: What is life … without time marking? *Biochim Biophys Acta BBA - Bioenerg*. 2025;1866(2):149542. doi:10.1016/j.bbabio.2025.149542